Draft version March 5, 2024
Preprint typeset using LaTeX style emulateapj v. 01/23/15

ADVANCED LIGO CONSTRAINTS ON NEUTRON STAR MERGERS AND R-PROCESS SITES

Benoit Côté,[1,2,8,9], Krzysztof Belczynski,[3] Chris L. Fryer,[4,9] Christian Ritter,[1,8,9]
Adam Paul,[1] Benjamin Wehmeyer,[5] Brian W. O'Shea[2,6,7,8]

Draft version March 5, 2024

ABSTRACT

The role of compact binary mergers as the main production site of r-process elements is investigated by combining stellar abundances of Eu observed in the Milky Way, galactic chemical evolution (GCE) simulations, binary population synthesis models, and Advanced LIGO gravitational wave measurements. We compiled and reviewed seven recent GCE studies to extract the frequency of neutron star - neutron star (NS-NS) mergers that is needed in order to reproduce the observed [Eu/Fe] vs [Fe/H] relationship. We used our simple chemical evolution code to explore the impact of different analytical delay-time distribution (DTD) functions for NS-NS mergers. We then combined our metallicity-dependent population synthesis models with our chemical evolution code to bring their predictions, for both NS-NS mergers and black hole - neutron star mergers, into a GCE context. Finally, we convolved our results with the cosmic star formation history to provide a direct comparison with current and upcoming Advanced LIGO measurements. When assuming that NS-NS mergers are the exclusive r-process sites, and that the ejected r-process mass per merger event is $0.01\,M_{\odot}$, the number of NS-NS mergers needed in GCE studies is about 10 times larger than what is predicted by standard population synthesis models. These two distinct fields can only be consistent with each other when assuming optimistic rates, massive NS-NS merger ejecta, and low Fe yields for massive stars. For now, population synthesis models and GCE simulations are in agreement with the current upper limit (O1) established by Advanced LIGO during their first run of observations. Upcoming measurements will provide an important constraint on the actual local NS-NS merger rate, will provide valuable insights on the plausibility of the GCE requirement, and will help to define whether or not compact binary mergers can be the dominant source of r-process elements in the Universe.

Subject headings: Binaries: close – Stars: abundances – Galaxy: evolution – Data: gravitational waves

1. INTRODUCTION

Understanding the production sites and the evolution of chemical elements in the Universe represents a significant challenge that requires a coherent effort between multiple fields, from nuclear physics to galaxy evolution and cosmological structure formation. Galactic chemical evolution (GCE, e.g., Chiappini et al. 2001; Gibson et al. 2003; Nomoto et al. 2013; Matteucci 2014) models and simulations are powerful tools to address this multidisciplinary topic, as they allow the astrophysical community to bridge the area of nuclear astrophysics (e.g., nucleosynthetic yields) and the observation of stellar abundances in local galaxies. They also provide valuable insights on how chemical species are mixed, recycled, and dispersed inside and outside galaxies, which ultimately leads to a better understanding of how galaxies form, evolve, and interact with their surrounding. In the recent years, an effort has been made to distinguish which site, between core-collapse supernovae (CC SNe) and neutron star - neutron star (NS-NS) mergers, is the dominant source of r-process elements (e.g., Argast et al. 2004; Wanajo & Ishimaru 2006; Arnould et al. 2007; Thielemann et al. 2011; Matteucci et al. 2014; Mennekens & Vanbeveren 2014; Cescutti et al. 2015; Wehmeyer et al. 2015). As described below, the purpose of this paper is to provide an additional constraint on this issue.

It is generally agreed that the presence of r-process elements, typically using the [Eu/Fe] ratio observed on the surface of extremely metal-poor stars with [Fe/H] $\lesssim -3$ in the Milky Way, is difficult to explain with NS-NS mergers alone, as the delay time needed between the formation of binary neutron stars and their coalescence prevents them from appearing before [Fe/H] ~ -2.5 (e.g., Argast et al. 2004; Matteucci et al. 2014; Cescutti et al. 2015; Wehmeyer et al. 2015). This suggested that CC SNe could be an important r-process source in the early Universe, as they would eject r-process elements and other lighter metals, such as Fe, simultaneously. However, in the last two years, more sophisticated studies using semi-analytical models and cosmological hydrodynamic simulations have shown that a reduced star formation efficiency in low-mass progenitor galaxies can slow

[1] Department of Physics and Astronomy, University of Victoria, Victoria, BC, V8W 2Y2, Canada
[2] National Superconducting Cyclotron Laboratory, Michigan State University, East Lansing, MI, 48824, USA
[3] Astronomical Observatory, Warsaw University, Al. Ujazdowskie 4, 00-478 Warsaw, Poland
[4] Computational Physics and Methods (CCS-2), LANL, Los Alamos, NM, 87545, USA
[5] Department of Physics, University of Basel, Klingelbergstrasse 82, CH-4056 Basel, Switzerland
[6] Department of Physics and Astronomy, Michigan State University, East Lansing, MI, 48824, USA
[7] Department of Computational Mathematics, Science and Engineering, Michigan State University, East Lansing, MI, 48824, USA
[8] Joint Institute for Nuclear Astrophysics - Center for the Evolution of the Elements, USA
[9] NuGrid Collaboration, http://nugridstars.org

down the early evolution of [Fe/H], which in turn allows NS-NS mergers to appear at [Fe/H] < -3 (e.g., Hirai et al. 2015; Komiya & Shigeyama 2016). This has also been seen in the one-zone models of Ishimaru et al. (2015). Furthermore, Shen et al. (2015) showed that non-uniform mixing in zoom-in cosmological hydrodynamic simulations, which generates scatter in the age−metallicity relationship, can push the appearance of NS-NS mergers to lower [Fe/H] values compared to simpler models (see also van de Voort et al. 2015).

As a summary, it appears that NS-NS mergers alone could explain the evolution of r-process elements when using a proper treatment of how galaxies assemble and how metals mix with primordial gas in the early Universe. It is therefore difficult to evaluate the relative contribution of CC SNe and NS-NS mergers based only on the appearance of NS-NS mergers on the [Fe/H] axis. In addition, in order to validate the conclusions drawn by GCE studies, it is important to combine numerical predictions with additional constraints that are not directly related to chemical evolution. Otherwise, when stellar abundances are the only constraint, it can be difficult to distinguish between reliable and misleading conclusions (see Côté et al. 2016c). Here are a few examples of additional observations that can be used by GCE studies – gas content (e.g, Kubryk et al. 2015), galactic inflow and outflow rates (e.g., Martin 1999; Lehner & Howk 2011), star formation efficiencies (e.g., Leroy et al. 2008), and galactic structure and dynamics (e.g., Minchev et al. 2013, 2014).

To constrain NS-NS mergers, the merger rates adopted in GCE studies can be compared to the merger rates predicted by population synthesis models (e.g., Dominik et al. 2012) and by observations of short gamma-ray bursts (e.g., Abadie et al. 2010). In addition, the LIGO (e.g., Abbott et al. 2009) and Advanced LIGO (e.g., Aasi et al. 2015) gravitational wave detectors have recently opened a new window for improving our understanding of compact binary mergers. The coalescence of two black holes has been detected (Abbott et al. 2016a) and measurements are currently ongoing to derive the rate of NS-NS mergers and black hole - neutron star (BH-NS) mergers (Abbott et al. 2016b). These upcoming measurement will provide solid constraints that, combined with chemical evolution models and simulations, will help defining whether or not NS-NS mergers can be the dominant source of r-process elements in the Milky Way and in its satellite galaxies. The LIGO horizon extends up to a redshift of 0.7 for the most massive black hole - black hole (BH-BH) mergers. However, for NS-NS and BH-NS mergers, we can expect a reduced horizon. We also note that merger rates can be derived from geological ^{244}Pu abundances (Hotokezaka et al. 2015). The mass ejected by NS-NS mergers can be constrained by relativistic hydrodynamic simulations (see Section 2.1.1) and from the scatter observed in the abundances of extremely metal-poor stars (Macias & Ramirez-Ruiz 2016).

In this paper, we aim to improve our understanding regarding the role of compact binary mergers in the production of the r-process by creating connections between GCE, population synthesis models, and Advanced LIGO measurements. Using interdisciplinary constraints and accounting for various sources of uncertainties, we systematically compare seven recent chemical evolution studies, which range from simple one-zone models to cosmological hydrodynamic zoom-in simulations, and homogenize the number of NS-NS mergers required to reproduce the observed abundances of Eu in the Milky Way. We also use our own simple chemical evolution model to explore different delay-time distribution (DTD) functions, including the metallicity-dependent ones predicted by population synthesis models, to see how they impact our ability to reproduce observations. We provide GCE predictions for both NS-NS and BH-NS mergers. The ultimate goal is to determine whether or not the binary merger rates needed in GCE simulations are reasonable and consistent with the upcoming Advanced LIGO measurements and population synthesis predictions.

This paper is organized as follows. In Section 2, we present the basic ingredients for implementing compact binary mergers in chemical evolution studies. In Section 3, we present seven recent GCE studies found in the literature, describe our own chemical evolution code, and provide an normalized comparison for the needed number of NS-NS mergers per unit of stellar mass formed. We explore, in Section 4, the impact of different analytical DTD functions for NS-NS mergers. In Section 5, we present our population synthesis models and include their predicted DTD functions and merger frequencies, for NS-NS and BH-NS mergers, into our chemical evolution code as an input. We convolved, in Section 6, the merger rates and frequencies needed in GCE studies and predicted by population synthesis models with the cosmic star formation history to allow a direct comparison with Advanced LIGO measurements. Our discussion and conclusions are presented in Sections 7 and 8, respectively.

2. IMPLEMENTATION OF BINARY MERGERS

In the following sections, we describe how to implement r-process production sites in GCE studies (see also Matteucci et al. 2014; Cescutti et al. 2015). The approach is similar to the implementation of Type Ia SNe and can be used for NS-NS and BH-NS mergers and for CC SNe. However, because of the purpose of this paper, we mainly focus on compact-binary mergers.

2.1. *Total Mass Ejected*

The total mass ejected by each binary merger allows us to scale the abundance pattern associated with the r-process and to determine the mass of heavy elements returned into the interstellar medium.

2.1.1. *Neutron Star Mergers*

Table 1 shows a compilation of the wide range of total mass ejected by NS-NS mergers, which is typically predicted by relativistic hydrodynamic simulations. In the models of Korobkin et al. (2012), the ejected masses range from ~ 0.008 to $\sim 0.04\,M_\odot$, but the most massive ejecta only occurs in peculiar progenitor mass ratios. In addition, the Newtonian smooth particle hydrodynamics simulations of Korobkin et al. (2012) possibly predict more ejecta than other calculations due to the lack of relativistic effects (Bauswein et al. 2013). Fryer et al. (2015) used the ejected masses found in Korobkin et al. (2012) and included them into population synthesis calculations. They found that although the upper limit for

TABLE 1
Compilation of Predicted Total Ejected Masses for Neutron Star Mergers

Reference	Ejected Mass [10^{-2} $M_\odot$]
Korobkin et al. (2012)	$0.76 - 3.9^a$
Bauswein et al. (2013)	$0.1 - 1.5$
Hotokezaka et al. (2013a)	$0.03 - 1.4$
Fryer et al. (2015)	$1.0 - 3.5^a$
Endrizzi et al. (2016)	$< 0.1 - 1.0$
Radice et al. (2016)	$0.02 - 12.5^a$
Sekiguchi et al. (2016)	$0.2 - 1.3$

[a] See text for discussion.

the ejected mass is around $0.035\,M_\odot$, the vast majority of NS-NS mergers should eject less than $0.02\,M_\odot$.

In addition to the dynamical ejecta mentioned above, outflows from the accretion disc of NS-NS mergers can also eject a considerable amount of material (e.g., Fernández & Metzger 2013; Fernández et al. 2015; Just et al. 2015). Although these outflows can be composed of r-process elements (e.g., Just et al. 2015; Wu et al. 2016), it is generally believed that disc outflows have a higher electron fraction (less neutron rich) than the dynamical ejecta. Several nucleosynthesis models argue that such ejecta only produces elements with atomic weights below 120-130 (e.g., Perego et al. 2014; Martin et al. 2015) and would therefore not contribute significantly to the evolution of Eu in our chemical evolution model.

One proposal to increase the ejecta of NS-NS mergers is to consider collisions instead of mergers, as the mass ejected in the case of highly eccentric binaries can be an order of magnitude larger than in the case of circular orbits. Radice et al. (2016), in their simulations, assumed parabolic orbits and ranged the periastron of these orbits to determine the mass of the ejecta. These parabolic orbits are produced in dense clusters with close encounters of compact objects, which are typically described in terms of impact separations (impact parameter) and velocities. In their simulations, the most massive ejecta only occurred for eccentric orbits with periastron distances below ~ 15 km. However, dynamical interactions producing such close orbits are rare and, overall, these systems are not expected to contribute significantly to the production of r-process material (see Appendix A).

Attempts to observe macronova candidates have discovered two possible candidates: GRB 130603B (Tanvir et al. 2013; Berger et al. 2013) and GRB 060614 (Jin et al. 2015; Yang et al. 2015). However, the nearby short burst GRB 150101B (Fong et al. 2016) places upper limits on the near infrared emission below these purported detections. On top of this, recent calculations of the opacities of the r-process elements produced in r-process ejecta argue that this ejecta is not bright in the near-IR (Fontes et al. 2015). These opacity arguments suggest that the emission observed from GRB 130603B and GRB 060614 cannot be from heavy r-process ejecta. Either the emission of these two bursts arises from wind ejecta (and hence does not measure the r-process ejecta) or these are false detections. In either case, there is no longer any evidence for dynamical ejecta masses above those produced in simulations.

The total mass ejected by NS-NS mergers seems to converge toward a value that is below $0.02\,M_\odot$, but the range is still very uncertain. To highlight this uncertainty, we consider in this study that NS-NS mergers can eject, on average, a total mass between 0.001 and $0.025\,M_\odot$, with a fiducial value of $0.01\,M_\odot$.

2.1.2. *Black Hole - Neutron Star Mergers*

BH-NS mergers could potentially produce more ejecta than NS-NS mergers. The work of Kawaguchi et al. (2015) suggests that the ejected mass can range between less than 10^{-4} up to $7.9 \times 10^{-2}\,M_\odot$. The total mass ejected by BH-NS mergers is sensitive to the spin of the companion black hole. According to Bauswein et al. (2014), the ejecta from a binary merger involving a non-rotating black hole ranges from 2×10^{-6} to $4 \times 10^{-4}\,M_\odot$, while the ejecta is increased up to 8.6×10^{-2} and $9.6 \times 10^{-2}\,M_\odot$ with fast rotating black holes. In addition, the mass ejected by BH-NS mergers also depends on the still unknown equation of state of neutron stars (Hotokezaka et al. 2013b). However, the rates of BH-NS mergers are typically lower than NS-NS mergers (see Section 5).

Having or not a mass ejection in BH-NS mergers is determined by orbital parameters at merger. In particular, if the tidal disruption distance between a neutron star and a black hole is smaller than the black hole event horizon, no mass ejection is expected. The extent of the black hole horizon depends sensitively on the spin of the black hole. The neutron star tidal disruption radius depends on the equation of state, the BH-NS mass ratio, and on the inclination of the neutron star's orbit with respect to the black hole spin. It was estimated that for highly spinning black holes, about 40% of BH-NS mergers lead to the disruption of the neutron star outside the black hole horizon, and therefore to mass ejection. However, for slow spinning black holes, neutron star disruptions outside the horizon is only expected to occur in $\sim$ 2% of the BH-NS mergers (Belczynski et al. 2008b).

2.2. *R-Process Yields*

Once the total mass ejected per r-process event is known, yields for heavy elements need to be selected in order to calculate the ejected mass of individual elements. Theoretical r-process nucleosynthetic calculations are making progress for compact binary mergers (Korobkin et al. 2012; Rosswog et al. 2014; Lippuner & Roberts 2015; Just et al. 2015; Roberts et al. 2016) and CC SNe (e.g., Arcones & Martínez-Pinedo 2011; Arcones & Thielemann 2013; Nakamura et al. 2015; Nishimura et al. 2015). Those yields can be used in chemical evolution models to probe the relative contribution of different production sites. However, those nucleosynthetic calculations, especially for Eu, are subject to many sources of uncertainties which are currently affecting the reliability of GCE predictions. Among others, nuclear masses can induce significant uncertainties in the predicted yields (Martin et al. 2016; Mumpower et al. 2016) while different fission models can change their abundance patterns (Korobkin et al. 2012; Goriely 2015; Eichler et al. 2016).

To reduce the uncertainties in this work, we adopt the observed r-process yields extracted using the solar r-process residuals method (Arnould et al. 2007), which implies a Eu mass fraction of 10^{-3} for each r-process event. Although the use of empirical yields prevents us

from drawing conclusions on how the r-process elements are made, we believe it is a good choice for the purpose of this paper. Our goal is to investigate whether or not NS-NS and BH-NS mergers are frequent enough to be able to reproduce the abundances of Eu observed in stars, assuming that compact binary mergers generate the r-process abundances pattern.

2.3. *Delay-Time Distribution Function*

The DTD function defines how many r-process events occur as a function of time in a given stellar population. If the r-process originates from CC SNe, the DTD function is therefore linked to the SN rate, which is defined by the initial mass function (IMF) and the lifetime of massive stars. If the r-process originates from compact binary mergers, the DTD function accounts for the delay needed between star formation, the formation of neutron stars and black holes, and the coalescence timescale of compact binary systems. In this last case, the DTD function can be seen as the probability for a binary system to merger as a function of time. In all cases, the merger rates are affected by the assumed binary fraction among the massive stars. As described in the next sections, many forms of DTD function can be used in GCE studies, from simple analytical prescriptions to DTD functions predicted by population synthesis models (e.g., Dominik et al. 2012).

As for the total mass ejected per r-process event, the normalisation of the DTD functions allows to scale the total amount of material returned into the interstellar medium. In our work, this normalisation parameter is described in units of number of r-process events per stellar mass formed, which represents the total number of NS-NS or BH-NS mergers that will occur during the lifetime of a stellar population.

3. GALACTIC CHEMICAL EVOLUTION STUDIES

Several GCE studies, which are reviewed in the next sections, have recently been conducted to determine if NS-NS mergers can be the dominant source of r-process in the Universe. Those studies usually aim to reproduce the abundance evolution of Eu (and sometimes other heavy elements, Argast et al. 2004; Cescutti et al. 2015; Ishimaru et al. 2015; Komiya & Shigeyama 2016) observed in the Milky Way. Conclusions are typically based on whether or not NS-NS mergers can occur early enough to explain the evolution of our Galaxy at low [Fe/H]. However, as explained in Section 1, the evolution of Eu in the early Universe is sensitive to the choice of code implementation and on how mass assembly is treated. In the present study, we complement the previous works by investigating the role of NS-NS mergers based on the total number of merger events needed in GCE simulations. As shown in Sections 5 and 6, this number can directly be compared with population synthesis models and Advanced LIGO measurements.

In the following sections, we briefly describe the chemical evolution codes used in different studies found in the literature. The extracted total number of NS-NS mergers per stellar mass formed, for all studies including ours, are shown in the upper panel of Figure 1. To provide a more reliable comparison between the different studies (see Section 3.9), we also show, in the middle and lower panels, the mass of Eu ejected per NS-NS merger event and the mass of Fe ejected by massive stars per stellar mass formed. The work of van de Voort et al. 2015 included neutron star mergers, but only considered the total ejected mass of r-process material. Therefore, in order to provide a consistent comparison among our selection of studies, which includes a normalization of Eu yields (see Section 3.9), we decided to exclude this study from our sample. The work of van de Voort et al. (2015), however, is important for the interpretation of our results and is considered in Section 4.2.

To be consistent with previous studies, we first focus on NS-NS mergers, but we include the contribution of BH-NS mergers in Section 5. We note that, for each selected study, we only considered the input parameters that generated the best agreement with observations. We recall that some of the studies reviewed in the following sections did include CC SNe as well as NS-NS mergers as sources of r-process elements. For those studies, we only considered the cases where NS-NS mergers were the exclusive r-process site. In several studies, which include ours, the binary fraction for massive stars is not specified, as it is indirectly included in the normalization parameters regulating the merger rates.

3.1. *Matteucci et al. (2014)*

Matteucci et al. (2014, M14) used a recent version of the two-infall model originally developed by Chiappini et al. (1997, 2001). It consists of a multi-zone model where the star formation rate is self-generated across the Galactic radius and calculated from a gas density profile, which evolves over time. The choice of stellar yields is the same as in the model 15 of Romano et al. (2010).

M14 assume that each NS-NS merger event ejects $3 \times 10^{-6}\,M_{\odot}$ of Eu. For each stellar population, the rate of NS-NS mergers follows the rate of appearance of neutron stars, which is linked to the lifetimes of massive stars. A constant delay is then added to the NS-NS merger rate in order to account for the time needed for neutron star binaries to coalesce. They adopted the IMF of Scalo (1986) with a lower[10] and upper mass boundaries of 0.1 and $100\,M_{\odot}$. A fraction of 1.8 % of all stars with initial mass between 9 and $30\,M_{\odot}$ are assumed to be the progenitors of NS-NS mergers. With this setup, we derived a total number of 4.34×10^{-5} NS-NS merger per unit of stellar mass formed.

The stellar yields of massive stars are taken from Kobayashi et al. (2006, K06), which includes 7 masses between 13 and $40\,M_{\odot}$ and 4 metallicities. All stars with initial mass equal or above $20\,M_{\odot}$ undergo a hypernova. According to Romano et al. (2010), massive star yields are applied to stars in the mass range of 8 to $100\,M_{\odot}$. All stars with an initial mass above $40\,M_{\odot}$ are assumed to eject the same material than the $40\,M_{\odot}$ models. A linear interpolation is performed between 6 and $13\,M_{\odot}$, where $6\,M_{\odot}$ represents the most massive asymptotic giant branch (AGB) models of Karakas (2010). After interpolating the models of Karakas (2010) to provide the same metallicities as in K06, we found that $2.84 \times 10^{-4}\,M_{\odot}$ of Fe is ejected in total per unit of stellar mass formed. We associated the lowest metallicity of provided by Karakas (2010), $Z = 0.0001$ in mass frac-

[10] We note that we found the lower limit in Romano et al. (2010).

tion, to the zero-metallicity yields of K06, which yielded similar results as when assuming no Fe ejecta for AGB stars at $Z = 0$.

3.2. *Cescutti et al. (2015)*

Cescutti et al. (2015, C15) used an inhomogeneous chemical evolution model that originates from the work of Cescutti (2008) and Chiappini et al. (2008), who aimed to reproduce metal-poor stars. In order to follow the stochasticity at early time, the Galactic halo has been split into several independent cells in which the IMF was randomly sampled, following an infall-driven star formation rate.

On average, each NS-NS merger is assumed to eject $5\times10^{-6}\,M_\odot$ of Eu. C15 considered that 2 % of all massive stars are part of binary systems that eventually produce a NS-NS merger. As in M14, the rate of NS-NS mergers follows the rate of CC SNe, but is delayed by a constant coalescence timescale. The adopted IMF is the one of Scalo (1986) with a lower and upper mass boundaries of 0.1 and $100\,M_\odot$. With a minimum mass of $8\,M_\odot$ for massive stars, we have calculated that 3.56×10^{-5} NS-NS merger occur per unit of stellar mass formed. The core-collapse Fe yields presented in François et al. (2004) are applied to all stars between 8 and $100\,M_\odot$. From the IMF properties, we found that massive stars eject $3.83\times10^{-4}\,M_\odot$ of Fe per stellar mass formed.

3.3. *Hirai et al. (2015)*

Hirai et al. (2015, H15) performed a series of hydrodynamic simulations of dwarf spheroidal galaxies, using the ASURA code described in Saitoh et al. (2008, 2009), to represent the building blocks of the Galactic halo.

The mass of Eu ejected by each NS-NS merger has been set to $2\times10^{-5}\,M_\odot$ (private communication) in order to reach the desired level of [Eu/Fe] = 0.5 at [Fe/H] = 0.0. We note that H15 did not include Type Ia SNe (SNe Ia) in their simulations, as the goal of their paper was to address the Eu abundances observed in extremely metal-poor stars (at [Fe/H] $\lesssim -3$). The IMF of Salpeter (1995) is considered with a lower and upper mass boundaries of 0.1 and $100\,M_\odot$. With the assumption that 1 % of all stars in the mass range between 8 and $20\,M_\odot$ produce NS-NS mergers, we derive a total of 5.45×10^{-5} NS-NS merger per unit of stellar mass formed. The stellar yields of K06 are applied to stars with an initial mass between 8 and $40\,M_\odot$. With the IMF used in H15, we calculated that, on average, $5.71\times10^{-4}\,M_\odot$ of Fe is ejected per unit of stellar mass formed.

3.4. *Ishimaru et al. (2015)*

Ishimaru et al. (2015, I15) used a one-zone model based on the originally work of Ishimaru & Wanajo (1999) and Ishimaru et al. (2004), which assumes homogeneous mixing. It has been designed to follow the chemical evolution of the building block galaxies that should have formed the Galactic halo. Several star formation and galactic outflow efficiencies have been explored in I15.

In their simulations, each NS-NS merger ejects $2\times10^{-5}\,M_\odot$ of Eu. In total, there are 500 times more core-collapse SNe than NS-NS mergers. According to Ishimaru & Wanajo (1999), the adopted IMF is the one of Salpeter (1995) with a lower and upper mass boundaries of 0.05 and $60\,M_\odot$. Stars with initial mass between 8 and $10\,M_\odot$ do not eject Fe, but are still expected to generate a core-collapse SN. From this setup, we find that 1.12×10^{-5} NS-NS merger occur per unit of stellar mass formed. This number, however, does not exactly match the cumulated number of NS-NS mergers presented in the Figure 1a of I15. Our calculation only becomes consistent if we assume that the final stellar masses given in I15 are corrected for stellar ejecta. If our assumption is valid, our value is in agreement when we assume that $\sim$ 40 % of the mass of a stellar population is returned into the interstellar medium. An alternative could be that I15 do not use the same IMF properties than what is described in Ishimaru & Wanajo (1999). We therefore cannot confirm that our derivation for the number of NS-NS mergers is correct for this study.

I15 used the stellar yields of K06 for stars more massive than $10\,M_\odot$. Following the IMF described above, we

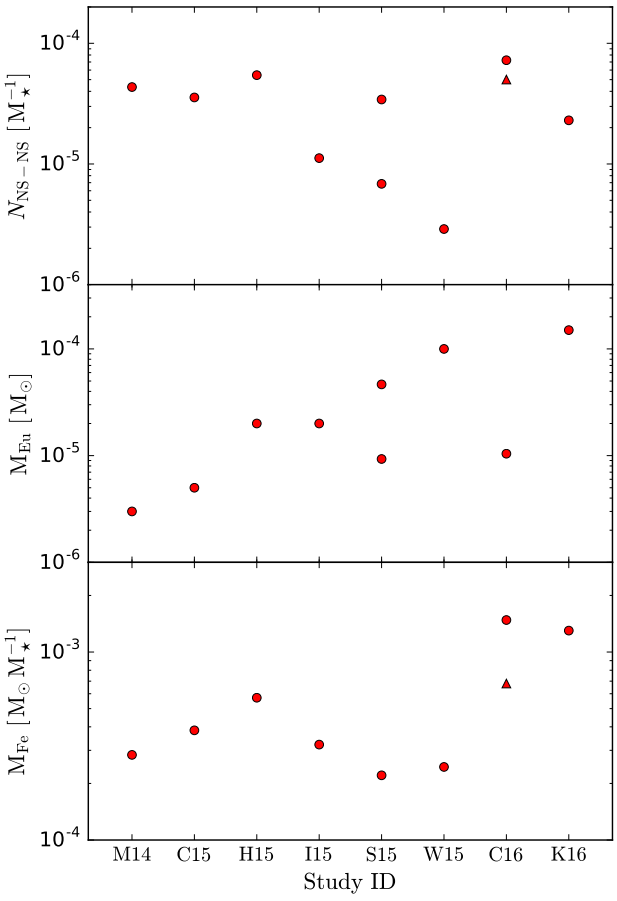

FIG. 1.— Number of NS-NS mergers (upper panel), per unit of stellar mass formed, extracted from different chemical evolution studies. The middle and lower panels show, respectively, the adopted mass of Eu ejected per NS-NS merger event and the average mass of Fe ejected by massive stars per stellar mass formed. Our study is labeled as C16. The other studies taken from the literature are Matteucci et al. (2014, M14), Cescutti et al. (2015, C15), Hirai et al. (2015, H15), Ishimaru et al. (2015, I15), Shen et al. (2015, S15), Wehmeyer et al. (2015, W15), and Komiya & Shigeyama (2016, K16). In our study (C16), the triangles and circles show, respectively, our results using the stellar yields calculated by Kobayashi et al. (2006) and by West & Heger (in preparation) and NuGrid.

found that 3.22×10^{-4} M$_\odot$ of Fe is ejected on average per unit of stellar mass formed. We note that extrapolating the models of K06 to cover the mass regime between 10 and 13 M$_\odot$ generate a similar result than simply applying the yields of the 13 M$_\odot$ model to all stars in that mass regime.

3.5. *Shen et al. (2015)*

Shen et al. (2015, S15) post-processed the Eris cosmological hydrodynamic zoom-in simulation (Guedes et al. 2011) in order to include the contribution of NS-NS mergers. They assumed that each NS-NS merger ejecta has a Eu mass fraction of 9.3×10^{-4}, following Sneden et al. (2008). With an r-process ejected mass of either 0.01 or 0.05 M$_\odot$, each NS-NS merger event ejects 9.3×10^{-6} or 4.65×10^{-5} M$_\odot$ of Eu, respectively. In total, 1.88×10^6 and 3.76×10^5 NS-NS mergers, depending to the adopted NS-NS merger ejected mass, are required in order to reproduce the solar Eu to O abundance ratio. In order to recover the number NS-NS mergers per unit of stellar mass formed, we first needed to recover the total amount of stars formed throughout the Eris simulation.

At redshift zero, according to Guedes et al. (2011), the stellar mass is 3.9×10^{10} M$_\odot$, which includes the stellar remnants. The relation between the initial stellar mass and the total ejected mass for massive stars is taken from Raiteri et al. (1996), while the one for stars between 1 and 8 M$_\odot$ is extracted from Weidemann (1987). Using the IMF of Kroupa et al. (1993) with a lower and upper mass boundaries of 0.08 and 100 M$_\odot$ (Raiteri et al. 1996), and the assumption that only stars between 1 and 40 M$_\odot$ contribute to the stellar ejecta (Stinson et al. 2006), we calculate that 29.1 % of the mass of a stellar population is returned into the interstellar medium. If we assume that the bulk of the stellar mass at redshift zero is composed of evolved stellar populations, 5.49×10^{10} M$_\odot$ of stars should be formed in total during the simulation. The number of NS-NS mergers per unit of stellar mass formed should then be 3.42×10^{-5} when NS-NS mergers eject 0.01 M$_\odot$ of r-process material, and 6.85×10^{-6} when they eject 0.05 M$_\odot$.

For the Fe yields of massive stars, S15 use the relation found in Raiteri et al. 1996 which is derived from the models of Woosley & Weaver (1995). Using the same IMF properties described above, we found that 2.21×10^{-4} M$_\odot$ of Fe is ejected per unit of stellar mass formed.

3.6. *Wehmeyer et al. (2015)*

Wehmeyer et al. (2015, W15) used an inhomogeneous chemical evolution model originally designed by Argast et al. (2004). A $(2\,\mathrm{kpc})^3$ simulation cube representing a portion of the Galaxy is split into 64 000 cells where stars can form to produce a blast-wave that pollutes neighbouring cells with heavy elements. When a star-forming region is selected, the mass of the stars are chosen randomly according to the adopted IMF.

Each NS-NS merger event is assumed to eject 10^{-4} M$_\odot$ of Eu. The number of NS-NS mergers that occur during the simulation is defined by $P_{\mathrm{NSM}} = 4 \times 10^{-4}$, which represents the probability of a newly born massive star to be in a binary system leading to a NS-NS merger event (or the frequency of NS-NS merger per number of massive star formed). Once the progenitor stars have undergone a CC SN and left behind a neutron star, the binary systems merge after one fixed, constant coalescence time. W15 uses the IMF of Salpeter (1995) with a lower and upper mass boundaries of 0.1 and 50 M$_\odot$. Given a minimum initial mass of 8 M$_\odot$ for massive stars, there is then in total 2.89×10^{-6} NS-NS merger per unit of stellar mass formed.

The stellar yields of massive stars are taken from the models of Thielemann et al. (1996) and Nomoto et al. (1997) and are applied to stars with initial mass between 10 and 50 M$_\odot$. In total, according to our calculation, 2.45×10^{-4} M$_\odot$ of Fe is ejected per unit of stellar mass formed, following the IMF described above.

3.7. *Komiya & Shigeyama (2016)*

Komiya & Shigeyama (2016, K16) used a semi-analytical model of galaxy formation and evolution, described in Komiya et al. (2014), to follow in a cosmological context the evolution of Eu in the Milky Way. Their model considers the impact of galactic outflows and high-velocity NS-NS merger ejecta on the pre-enrichment of neighbouring proto-galaxies, which eventually become part of the Milky Way. In each stellar population, NS-NS mergers appear following a delay-time distribution function in the form of t^{-1} with a lower and upper time boundaries of 10 Myr and 10 Gyr, a choice motivated by Dominik et al. (2012).

They assume that each NS-NS merger ejects 1.5×10^{-4} M$_\odot$ of Eu. The adopted IMF (see their equation 2) has a similar shape than the one of Chabrier (2003), but with different parameters to better reproduce the metallicity distribution function of metal-poor stars. The lower and upper mass boundaries are 0.08 and 100 M$_\odot$, where only stars in the mass range between 8 and 25 M$_\odot$ are candidate progenitors for NS-NS mergers. With a binary fraction of 50 % with a flat mass ratio distribution for primary and secondary stars, and the assumption that only 1 % of the candidate binaries produce NS-NS mergers, there is 2.30×10^{-5} NS-NS merger occuring per unit of stellar mass formed (private communication). For core-collapse SNe, the stellar yields of K06 are applied to stars with initial mass between 10 and 40 M$_\odot$ with a hypernova fraction of 0.5 for stars more massive than 20 M$_\odot$ (Komiya et al. 2014). With their IMF, we calculated that 1.26×10^{-3} M$_\odot$ of Fe is ejected on average by massive stars.

3.8. *This Study*

`OMEGA`[11] is a one-zone chemical evolution model that assumes uniform mixing and includes several prescriptions for galactic inflows and outflows (Côté et al. 2016c). It uses an input star formation history, along with different star formation efficiency parameterizations, to mimic the evolution of observed and simulated galaxies. Each stellar population represents a complete sample of the IMF.

For massive stars, we test the yields found in K06 as well as the ones calculated by NuGrid[12] (Pignatari et al. 2016; C. Ritter et al. in preparation) with the delayed remnant mass prescription described in Fryer et

[11] https://github.com/NuGrid/NuPyCEE
[12] http://nugridstars.org/data-and-software/yields/set-1

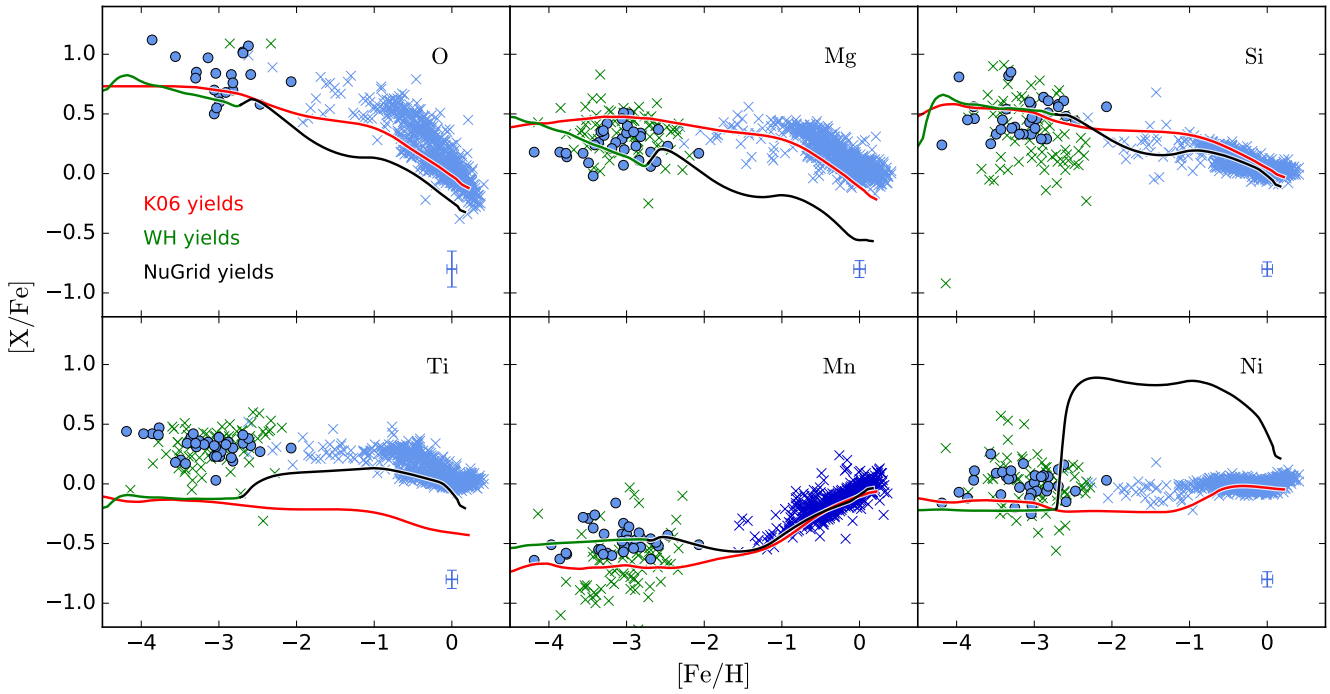

FIG. 2.— Predicted chemical evolution of six light elements using the yields calculated by Kobayashi et al. (2006, red lines), West & Heger (in preparation, green lines), and NuGrid (black lines). Observational data come from Cayrel et al. (2004, light blue circles), Cohen et al. (2013, green crosses), Bensby et al. (2014, light blue crosses), and Battistini & Bensby (2015, dark blue crosses). The error bar symbol on the lower-right corner of each panel represents the average error of all data.

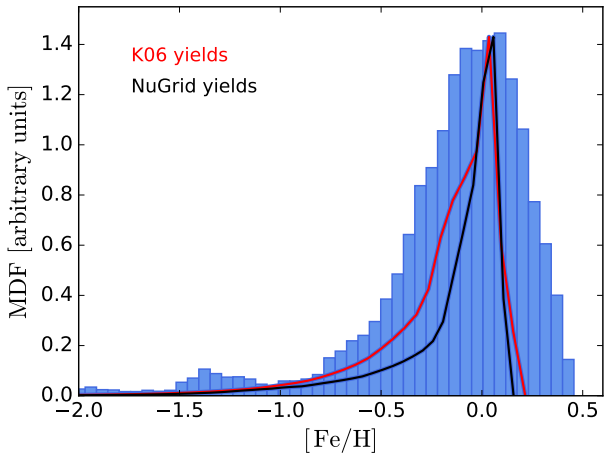

FIG. 3.— Predicted metallicity distribution function using the yields calculated by Kobayashi et al. (2006, red line) and NuGrid (black line). The blue histogram has been extracted from APOGEE R12 data and the ASPCAP reduction pipeline (García Pérez et al. 2016).

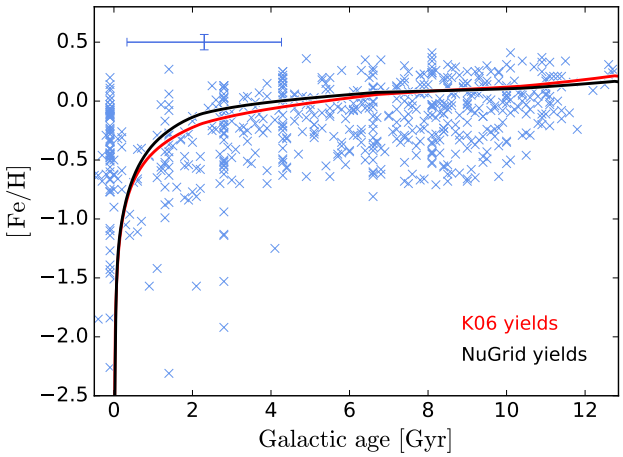

FIG. 4.— Predicted evolution of [Fe/H] as a function of Galactic age using the yields calculated by Kobayashi et al. (2006, red line) and NuGrid (black line). Observational data come from (Bensby et al. 2014, blue crosses) where the error bar symbol on the top-left corner represents the average error of all data. The error in the age measurements is typically larger for older stars. Although our one-zone model cannot distinguish between the different Galactic structures, the observational data include halo and disk stars.

al. 2012. We supplement NuGrid yields with the zero-metallicity yields calculated by West & Heger (HW, in preparation) with the minimum fallback prescription (see Côté et al. 2016b). The yields of low- and intermediate-mass stars are provided by NuGrid. We use the IMF of Chabrier (2003), with a lower and upper mass boundaries of 0.1 and 100 $M_\odot$, and consider that massive stars only contribute to the chemical enrichment when their initial mass is between 8 and 30 $M_\odot$ (see discussion in Côté et al. 2016a). Under these assumptions, 6.80×10^{-4} and 1.48×10^{-3} $M_\odot$ of Fe is ejected on average per unit of stellar mass formed when using K06 and NuGrid yields, respectively. For SNe Ia, we use the yields of Thielemann et al. (1986) and the delay-time distribution function described in Côté et al. (2016a).

In this study, we use the galaxy modeling assumptions described in Côté et al. (2016b) to model the Milky Way. Figure 2 shows our numerical predictions for six light elements. As also shown in Romano et al. (2010)

and in Mollá et al. (2015), the choice of stellar yields plays a fundamental role in galactic chemical evolution models. The breaks seen in the green and black lines at [Fe/H] ~ -2.7, represent the transition between the zero-metallicity yields of WH (green) and the non-zero metallicity yields of NuGrid (black). The discontinuities occur because these two sets of yields have not been calculated with the same code and modeling assumptions, as opposed to K06 yields, which include both zero- and non-zero-metallicity stellar models. The high [Ni/Fe] abundances predicted using NuGrid yields are caused by an α-rich freezout component that is included in the ejecta of some of the CC SN models. Such Ni-rich components are not present in the yields of WH and K06, which explains the significant difference seen in the evolution of [Ni/Fe] when using NuGrid yields (see Figure 2). This discrepancy is mostly due to the stellar remnant mass prescriptions adopted by NuGrid for massive stars. Those prescriptions are designed to reproduce the neutron star and black hole mass distribution function observed in the Milky Way and therefore generate relatively low remnant masses for their 12 and 15 $M_\odot$ stellar models (Fryer et al. 2012; Pignatari et al. 2016).

For each tested set of yields, we tuned independently mass of gas at early and late times to reproduce the current gas fraction observed in the Milky Way and to ensure that SNe Ia appear at [Fe/H] ~ -1 (see Côté et al. 2016b for more details). We also tuned the strength of galactic outflows to ensure that our predicted metallicity distribution function (MDFs[13]) peaks at [Fe/H] ~ 0 (see Figure 3). Because NuGrid yields eject more Fe than K06 yields, stronger outflows are needed with NuGrid yields in order to provide similar values for the peak of the MDF. With our model, this results in a flatter age−metallicity relation (see Figure 4) and thus a narrower MDF (see Figure 3).

We assume that each NS-NS merger event ejects $10^{-5}\,M_\odot$ of Eu, corresponding to a total ejected mass of r-process elements of $10^{-2}\,M_\odot$ with a Eu mass fraction of 10^{-3} (Arnould et al. 2007). In the next sections, we explore different DTD functions for NS-NS mergers. As will be shown in Section 4.1, the total number of NS-NS mergers per stellar mass formed needed to reproduce the observed Eu abundances in the Milky Way is 5.01×10^{-5} when using K06 yields, and 7.24×10^{-5} when using NuGrid yields (see Section 5 for uncertainties). For our study, C16, the circles and triangles shown in Figure 1 present our results using NuGrid and K06 yields, respectively.

3.9. *Normalized Comparison*

As shown in the previous sections, different GCE models and simulations generally use different IMFs with different mass boundaries, different stellar yields, different progenitors for massive stars and NS-NS mergers, and different DTD functions and normalizations for the NS-NS merger rates. To provide a relevant comparison between the considered studies, we have corrected $N_{\rm NS-NS}$, the derived number of NS-NS mergers per unit of stellar mass formed, in order to normalize the studies to the same Eu and Fe yields. For each study, the normalized value, $N'_{\rm NS-NS}$, is given by

$$N'_{\rm NS-NS} = N_{\rm NS-NS}\left(\frac{M_{\rm Eu}}{M'_{\rm Eu}}\right)\left(\frac{M'_{\rm Fe}}{M_{\rm Fe}}\right), \qquad (1)$$

where $M_{\rm Fe}$ and $M_{\rm Eu}$ are the masses of Fe and Eu ejected by massive stars and NS-NS mergers, respectively, originally adopted in the study (see Figure 1). $M'_{\rm Fe}$ and $M'_{\rm Eu}$ represent the normalized yields common to all studies. Here we chose $M'_{\rm Fe} = 3.35\times10^{-4}\,M_\odot$, the median value of the $M_{\rm Fe}$ distribution, and $M'_{\rm Eu} = 10^{-5}\,M_\odot$, representing a Eu yield of 10^{-3} with a total mass of r-process ejecta of $10^{-2}\,M_\odot$. We refer to Section 5.4 for the error bars of our normalization.

This normalization is not complete, as it does not include corrections for different implementations of SNe Ia, which are significant contributors of Fe at [Fe/H] $\gtrsim -1$. Nevertheless, as shown in Figure 5, this normalization significantly reduces the level of scatter seen between the various studies, from a factor of ~ 25 (red symbols) down to a factor of ~ 4 (blue symbols). An additional correction has been applied to S15 and K16 since their [Eu/Fe] value at [Fe/H] $= 0$ was originally greater than zero. The normalized values, before the application of this additional correction, are shown as transparent blue circles. The range shown in blue in Figure 5 overlaps with the values derived from Eu abundances in ultra-faint dwarf galaxies (Beniamini et al. 2016).

Our work, C16, originally showed the highest value for $N_{\rm NS-NS}$ because we used the highest Fe yields (see lower panel of Figure 1). Therefore, compared to other studies, we needed more NS-NS mergers to counterbalance the Fe ejecta from massive stars. However, if we had used the

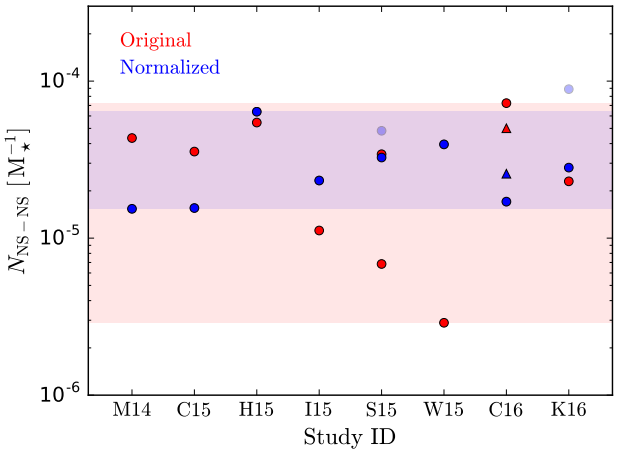

FIG. 5.— Number of NS-NS mergers, per unit of stellar mass formed, needed in different chemical evolution studies in order to reproduce the Eu abundances in the Milky Way. The red circles represent the original values extracted from each study while the blue circles show the normalized values as if all studies used the same mass of Eu ($10^{-5}\,M_\odot$) ejected per NS-NS merger event and the same mass of Fe ($3.35\times10^{-4}\,M_\odot$) ejected by massive stars per stellar mass formed. The red and blue shaded areas highlight the range of values given by the considered studies. S15 and K16 originally showed a final Eu abundances that was larger than the solar [Eu/Fe] composition. To be consistent with other studies, a correction factor has thus been applied to scale their final [Eu/Fe] ratios down to zero. The transparent blue circles represent the normalized values before the correction.

[13] Here, the metallicity distribution function represents the current the number of stars in the Milky Way having a certain [Fe/H] value in their atmosphere.

normalized $M'_{\rm Fe}$, which is lower than the original $M_{\rm Fe}$, less NS-NS mergers would have been necessary to reach the same Eu abundances. W15 originally showed the lowest value for $N_{\rm NS-NS}$ because they used one of the highest Eu yields (see middle panel of Figure 1) and one of the lowest Fe yields (see lower panel of Figure 1). This means W15 did not require as many NS-NS mergers as in other studies to each the same [Eu/Fe] ratios. By using lower Eu yields and larger Fe yields, $(M_{\rm Eu}/M'_{\rm Eu})$ and $(M'_{\rm Fe}/M_{\rm Fe})$ both become larger than 1, which increases the number of NS-NS mergers needed to reproduce the Eu abundances (see equation 1).

We refer to Section 7 for a discussion on different sources of uncertainties that can affect the normalization process.

4. ANALYTICAL DELAY-TIME DISTRIBUTIONS

In this section, we use `OMEGA` and explore different DTD functions commonly used for NS-NS mergers in GCE studies to investigate how they affect our ability to reproduce the global chemical evolution trend of Eu in the Milky Way. We recall that we focus on Eu in order to compare our results with the previous studies described in Section 3.

4.1. *Constant Coalescence Timescale*

Figure 6 shows our numerical predictions using constant coalescence timescales since star formation, $t_{\rm coal}$, after which all NS-NS mergers in a stellar population release their ejecta. As found by almost all previous studies, $t_{\rm coal}$ has an impact on when, or at which [Fe/H], NS-NS mergers first appear. The shape of our numerical predictions are similar to one generated by other models that either use a constant coalescence timescale (e.g., Argast et al. 2004; W15) or assume that all NS-NS mergers occur within a very short period of time (e.g., M14; C15). A bend in the evolution of [Eu/Fe] at [Fe/H] ~ -1 is clearly visible and originates from the iron ejected by SNe Ia. Furthermore, our results are consistent with the ones of M14 (see their Figure 2) in the sense that the coalescence timescale parameter can shift the appearance of NS-NS mergers on the [Fe/H] axis, but cannot change the [Eu/Fe] ratio at later times (see Figure 6). This conclusion, however, is only valid for relative short coalescence timescales. In Figure 6, the total number of NS-NS mergers per unit of stellar mass formed was 5.01×10^{-5} when using K06 yields and 7.24×10^{-5} when using NuGrid yields, for all chosen values for the coalescence timescale. All of the models cited in this paragraph, including ours, do not include hydrodynamics. We note, however, that H15 used constant coalescence timescales in their hydrodynamic simulations.

When $t_{\rm coal} = 100\,$Myr (dot-dashed lines in Figure 6), our NS-NS mergers appear at a [Fe/H] value that is similar to one found in M14. However, when $t_{\rm coal}$ is shorter, our NS-NS mergers tend to appear at lower [Fe/H] compared to M14. This can be caused by the fact that in M14, the coalescence timescale represents the time span between the CC SNe and NS-NS mergers events, whereas in our model it represents the time span between star formation and NS-NS mergers events. Alternatively, it can be caused by different gas and star formation efficiency treatments at early time. As a matter of fact, because

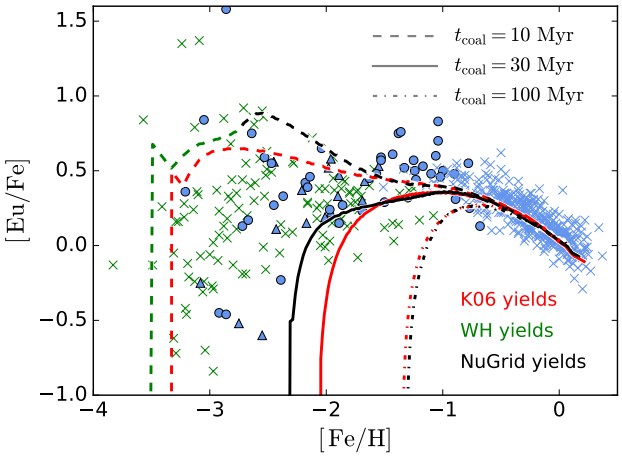

FIG. 6.— Predicted chemical evolution of Eu, for different constant coalescence timescales for NS-NS mergers (different line styles), using the yields calculated by Kobayashi et al. (2006, red lines), West & Heger (in preparation, green lines), and NuGrid (black lines). In this study, the constant coalescence timescale represents the delay between star formation and the appearance of all NS-NS mergers in a stellar population. Observational data come from Roederer et al. (2009, blue triangles), Hansen et al. (2012, blue circles) Roederer et al. (2014, green crosses), and Battistini & Bensby (2016, blue crosses).

of the abrupt slope of the age−metallicity relation when [Fe/H] is below −1 (see Figure 4), a slight delay in the enrichment process, or a slight modification of the enrichment efficiency, can induce a major change on when NS-NS mergers first appear on the [Fe/H] axis.

Many uncertainties are associated with the first Gyr of evolution in our model (e.g., very low-metallicity yields, star formation efficiency, gas content and metal mixing, and strength of galactic inflows and outflows). Furthermore, we do not think that our one-zone model is suited to reproduce the evolution of our Galaxy at early time. Stochastic processes and a proper treatment of how galaxies assemble in the early Universe through galaxy mergers is currently not included in `OMEGA` (but see our recent developments in Côté et al. 2016d). For this reason, we conclude that it is more reliable to use the total number of NS-NS mergers, rather than when they appear, to investigate whether or not NS-NS mergers can be the dominant source of r-process elements. This number can directly be compared with population synthesis models (see Section 5). In addition, as will be shown in Section 6.3, the predicted cosmic NS-NS merger rate density, which can be compared with upcoming Advanced LIGO measurements, is more sensitive to the total number of merger events than to the choice of the DTD function.

4.2. *Power Law Distribution*

A more realistic implementation is to assume that NS-NS mergers in a stellar population are distributed within several Gyr instead of occurring all after one fixed, constant coalescence time. Here we explore the delay-time distribution (DTD) function in the form of $t^{-\gamma}$ with a lower and upper time boundaries of 10 Myr and 10 Gyr. We refer to Section 5 for different forms. Figure 7 shows our numerical predictions using different values for the power-law index, γ. In all cases, we normalized the DTD

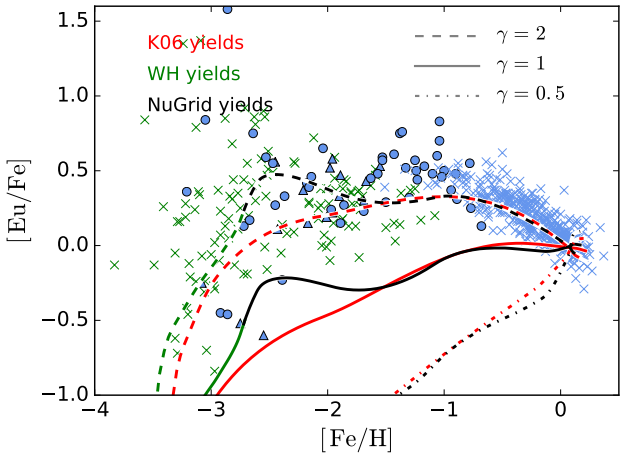

FIG. 7.— Same as Figure 6, but using a power-law delay-time distribution function for NS-NS mergers in the form of $t^{-\gamma}$, applied from 10 Myr to 10 Gyr, with different values for γ (different line styles).

functions to generate the same number of NS-NS mergers, per unit of stellar mass formed, as in Section 4.1. As shown in the last figure, our one-zone model cannot reproduce the Eu trend when $\gamma = 1$ (solid lines), which is, however, a value motivated by the work of Dominik et al. (2012). Our predictions are worst when $\gamma = 0.5$ (dot-dashed lines), since NS-NS mergers are further delayed compared to the case where $\gamma = 1$. We reasonably reproduce observations when $\gamma = 2.0$ (dashed lines), since this abruptly decreasing power-law brings our implementation closer to the constant coalescence timescale assumption (see Figure 6).

The small variations seen in Figure 7 at [Fe/H] > 0 are caused by different amount of Eu lost by galactic outflows, which are more powerful at the beginning of our simulations. More Eu is thus kept in the system when NS-NS mergers mainly occur at later times (dot-dashed lines).

4.2.1. *Non-Uniform Mixing*

As opposed to `OMEGA`, cosmological zoom-in hydrodynamic simulations (S15, van de Voort et al. 2015) and semi-analytical models of galaxy formation within a cosmological context (Komiya & Shigeyama 2016) can reproduce metal-poor stars, at least down to [Fe/H] ~ -3, with $\gamma = 1$. This highlights major differences between one-zone models and more sophisticated simulations. In particular, hydrodynamic simulations self-consistently follow the non-uniform mixing of metals at early time, which generates significant scatter in the age−metallicity relation (see also Kobayashi et al. 2011; H15). S15 compared their original results with an homogeneous-mixing version of their simulations, which is similar to our one-zone model. They found that Eu can only be recycled in very-low metallicity stars when stellar and NS-NS merger ejecta are not uniformly mixed within the galactic gas (see their Figure 7). However, non-uniform mixing is not the only important ingredient to consider in order to address the early evolution of our Galaxy. Inhomogeneous chemical evolution models, such as the ones of C15 and W15, still have difficulties to reproduce the Eu abundances at [Fe/H] $\lesssim -2$ with reasonable coalescence timescales when considering NS-NS merger as the exclusive r-process site.

4.2.2. *Cosmological Context*

Another reason why our one-zone model fails to reproduce the Eu trend at early time, when using a power law for the DTD function for NS-NS mergers with $\gamma = 1$ and 0.5, is because we ignore the hierarchical nature of how galaxies form in a cosmological context. One-zone models consider a single gas reservoir associated with one galaxy while in reality, massive galaxies such as the Milky Way are the results of many galaxy mergers (e.g., Vogelsberger et al. 2014; Schaye et al. 2015; Griffen et al. 2016). Within this framework, the early evolution of the Milky Way should therefore be represented by many low-mass progenitor galaxies.

Recently, H15 shown with hydrodynamic simulations that NS-NS mergers can enrich stars at [Fe/H] $\lesssim -3$ in dwarf galaxies when the star formation efficiency is lowered compared to more massive systems, which slows down the evolution of [Fe/H] at early time (see also I15). Although H15 assumed a constant coalescence timescale instead of a power law for the DTD function of NS-NS mergers, they were able to reproduce metal-poor stars even when no NS-NS merger occurred before 100 Myr (see their Figure 7). This is not possible with simpler models, as shown by the dot-dashed lines in our Figure 6 (see also Argast et al. 2004; M14; C15; W15). Komiya & Shigeyama (2016) also demonstrated, using a semi-analytical model within a cosmological context, that Ba and Eu are better reproduced with NS-NS mergers if the star formation efficiency decreases with the mass of progenitor galaxies.

4.2.3. *Shape of Numerical Predictions*

As shown in Figure 6 and 7, the shape of numerical predictions are different when assuming a constant coalescence timescale or a power law for the distribution of NS-NS mergers as a function of time. When using a power law with an index of -1 or -0.5, it is difficult to recover the knee observed at [Fe/H] ~ -1 in the evolution of Eu. Even if our GCE model is relatively simple, this lack of decreasing trend above this metallicity is also seen in the hydrodynamic simulations of S15. The knee is visible in the simulations of van de Voort et al. 2015, but only at [Fe/H] ~ 0. This difficulty is also reported by Komiya & Shigeyama (2016). On the other hand, the knee can easily be reproduced when using coalescence timescales after which all NS-NS mergers occur in a stellar population (see Figure 6 and M14; C15; W15). If NS-NS mergers are actually the main source of r-process elements, this suggests that NS-NS mergers need to occur on short timescales.

4.3. *Constraints for Neutron Star Mergers*

As discussed in the previous sections, it seems like non-uniform mixing and a proper treatment of how galaxies assemble in the early Universe are essential ingredients to reproduce low-metallicity stars and to understand how NS-NS merger ejecta can be recycled in the early stage of our Galaxy. However, at higher [Fe/H], GCE simulations in general are less sensitive to those aspects and simple models like `OMEGA` can provide valuable insights

(see also Figure 6 in S15). Although our one-zone model is not suited to reproduce metal-poor stars, our predictions always end roughly at [Eu/Fe] ~ 0, regardless of the choice of implementation for the delay of NS-NS mergers (see Figures 6 and 7). To constrain NS-NS mergers and investigate whether or not they can be the dominant source of r-process elements, we believe that the total number of neutron star mergers needed to ultimately reach [Eu/Fe] ~ 0 at [Fe/H] ~ 0 is a more robust and universal constraint than evaluating the capacity of models to reproduce metal-poor stars, as it is less affected by the various sources of uncertainty associated with the early evolution of our Galaxy.

5. POPULATION SYNTHESIS MODELS

Here we introduce our population synthesis models, present their predicted compact binary merger rates, and discuss their impact on GCE.

5.1. *Code Description*

Population synthesis calculations were performed using `StarTrack` (Belczynski et al. 2002, 2008a). This code has recently been improved for the evolution of massive stars. It now includes better assumptions for the evolution of the common envelope (CE) phase (Dominik et al. 2012), the masses of compact objects produced by CC SNe (Fryer et al. 2012; Belczynski et al. 2012), the initial conditions for stellar binaries (constrained by observations, de Mink & Belczynski 2015), and for the evolution of star formation and the average metallicity in the Universe (also constrained by observations, Belczynski et al. 2016b). This last improvement is used in Section 6 to predict the cosmic compact binary merger rate densities.

Our calculations are originally based on analytic fits made to the non-rotating stellar models presented in Hurley et al. (2000). However, we updated these models with revised stellar wind prescriptions (Vink 2011) and a new compact-object formation scheme (Fryer et al. 2012). We have begun calibrating our evolution with calculations performed with modern stellar models (Pavlovskii et al. 2016).

5.1.1. *Initial Setup*

All massive stars with a zero age main sequence mass ($M_{\rm ZAMS}$) greater than $7-10\,{\rm M}_\odot$ are assumed to be the progenitors of neutron stars and black holes. The initial parameters for massive stars in binary systems are guided by recent observations of O/B binaries (Sana et al. 2012; Kobulnicky et al. 2014). The mass of the primary stars is chosen from a three-component broken power-law initial mass function with an index of -2.3 for massive stars. A flat mass ratio distribution is used to calculate the mass of the secondary stars. Binaries are assumed to form predominantly on close and nearly circular orbits. We assume that the binary fraction is 100% for stars more massive than $10\,{\rm M}_\odot$ and 50% for less massive stars.

As mentioned above, the stellar models used in our study do not include the effects of rotation on their evolution. However, we include the impact of rotation with estimates of the tidal interactions between the stars and their binary orbit. We assume that our stars rotate at moderate velocities ($200-300$ km s^{-1}). We do not consider the small fraction of massive stars that may rotate at very high speeds (~ 600 km s^{-1}). For such rapidly rotating stars, the effects of rotation on their evolution need to be included in evolutionary calculations (Marchant et al. 2016; de Mink & Mandel 2016; Eldridge & Stanway 2016; Woosley 2016).

5.1.2. *Binary Evolution*

Stellar spins (and thus binary orbits) are affected by magnetic braking when stars have significant convective envelopes. Additionally, we account for the orbital changes due to the mass lost by stellar winds and angular momentum loss due to the emission of gravitational waves (important only for very compact binaries). The development and dynamical stability of the Roche lobe overflow (RLOF) is judged based on the following: binary mass ratio, evolutionary stage of the donor, response to mass loss, and behaviour of the orbital separation in response to mass transfer and angular momentum loss (Belczynski et al. 2008a).

During stable RLOF, we assume that half of the mass is accreted onto the companion, while the other half is lost from the binary with the specific angular momentum (we adopt the rather effective angular momentum loss with $j_{\rm loss} = 1.0$ defined in Podsiadlowski et al. 1992). Unstable mass transfer is assumed to lead to a CE. This is treated using the energy balance formalism with an effective conversion of orbital energy into envelope ejection ($\alpha = 1.0$). The envelope binding energy depends on the mass, radius, and metallicity of the donor star. During the CE phase, neutron stars and black holes accrete at 10% of the Bondi-Hoyle rate (Ricker & Taam 2008; Macleod & Ramirez-Ruiz 2015).

We account for mass loss, neutrino loss, and natal kicks during SNe. These explosions affect the binary orbits and can, for specific configurations, unbind and disrupt binary systems.

5.1.3. *Neutron Stars and Black Holes*

The mass of each compact object is based on a selection of hydrodynamical SN models that are initiated from detailed stellar evolutionary calculations (Woosley et al. 2002; Heger et al. 2003; Fryer 2006; Limongi & Chieffi 2006; Dessart et al. 2007; Poelarends et al. 2008; Young et al. 2009). The resulting mass of a compact object is based on the stellar mass at the time of core collapse and on the final mass of its carbon-oxygen core (Fryer et al. 2012). In this study, we use a rapid SN explosion prescription that reproduces the observed mass gap between neutron stars and black holes (Belczynski et al. 2012). Neutron stars are formed with masses in the range of $1.1-2.5\,{\rm M}_\odot$, while black holes form with masses in the range of $5-94\,{\rm M}_\odot$. The upper limit for the mass of a black hole is set by the strength of stellar winds and their dependence on metallicity (Belczynski 2010).

For single stars, with our formulation, there is a strict delimitation between neutron stars and black holes based on the ZAMS mass of the compact object progenitors. This mass threshold depends on metallicity and is found at $M_{\rm ZAMS} \approx 20\,{\rm M}_\odot$ for solar metallicity ($Z = 0.02$) progenitors. We note that binary interactions may significantly affect this limit. As a matter of fact, stars as massive as $100\,{\rm M}_\odot$ can form either neutron stars or black holes depending on their specific binary configurations

(Belczynski & Taam 2008). In other words, our simulations include non-monotonic formation of neutron stars and black holes with respect to progenitor initial mass, with neutron stars and black holes mixed up in a wide range of initial masses ($M_{\rm ZAMS} \approx 10-100\,{\rm M}_\odot$). This prescription has been designed to reproduce observations of compact objects.

5.1.4. *Selection of Models*

In this study, we use three models that were calculated and presented in Belczynski et al. (2016b), which are the standard model (M1), the optimistic model (M2), and a model with low natal kicks (M6). The standard model includes our best choices on the various parts of uncertain evolutionary physics as described above. In particular, the natal kicks for neutron stars and black holes are adopted from the velocity distribution measured for single pulsars in our Galaxy (Hobbs et al. 2005) – the natal kicks are drawn from a 1-D Maxwell distribution with dispersion of $\sigma = 265\,{\rm km\,s^{-1}}$ and an average 3-D speed of $\sim 400\,{\rm km\,s^{-1}}$. However, we lower the natal kick value according to the amount of fallback calculated for each compact object formation. For neutron stars, the amount of fallback is rather small and they receive high natal kicks. For very massive black holes ($\gtrsim 10\,{\rm M}_\odot$), all or almost all material falls back onto the black holes and thus receive no natal kick. For moderate mass black holes, the natal kick value is also moderate (Fryer et al. 2012).

In the standard model M1, we assume that stars that evolve through the Hertzsprung gap, mostly with radiative envelope, cannot survive a CE phase and merge before becoming double compact binaries (Belczynski et al. 2007). The two alternative models differ from the standard M1 model by only one aspect. In model M2, we allow Hertzsprung gap stars to initiate and a CE and to survive it. This effectively enhances the formation of all types of double compact object mergers (Belczynski et al. 2007, 2016b). In model M6, all compact objects, both neutron stars and black holes, receive a low natal kicks with $\sigma = 70\,{\rm km\,s^{-1}}$. We do not modify natal kicks with the fallback factor. This means that neutron stars receive on average smaller natal kicks while massive black holes receive larger natal kicks, compared to model M1.

Recent detailed evolutionary calculations seem to indicate that Hertzsprung gap stars should lead to a stable RLOF rather than to a CE (Pavlovskii et al. 2016). This scenario would thus lead to a larger number of non-merging compact objects compared to the M2 model. This is why we call the M2 model optimistic. Actually, in cases of very massive stars leading to black hole - black hole mergers, this model already appears be excluded by advanced LIGO measurements (Belczynski et al. 2016b). However, we cannot exclude yet the possibility that this M2 model is consistent for lower mass stars (neutron star progenitors), since our predicted cosmic NS-NS merger rate density for this model is $\sim 250\ {\rm Gpc^{-3}\ yr^{-1}}$ and is currently below the upper limits expected by advanced LIGO (see Section 6).

A more detailed study of extreme cases in population synthesis models will soon be conducted. Although our selection of models provides a view of the evolutionary uncertainties associated with the models described in Belczynski et al. (2016b), we warn that they are not representative of the entire range of plausible scenarios.

5.2. *Predicted Merger Rates*

Figure 8 shows the predicted merger rates using our optimistic (upper panels), standard (middle panels), and low natal kick (lower panels) models, for a stellar population with a total mass of $2.8 \times 10^8\,{\rm M}_\odot$. Although only three metallicities are presented in this last figure, the NS-NS (green lines), BH-NS (red lines), and BH-BH (black lines) merger rates have been calculated for 32 metallicities. At low metallicity, BH-NS and BH-BH mergers appear earlier than NS-NS mergers. This is because black holes typically have a larger mass at lower metallicities (Belczynski 2010), which leads to shorter merger times compared lighter-mass NS-NS systems (Peters 1964).

Figure 9 illustrates the total number of mergers per unit of stellar mass formed, which represents the normalization of the merger rates presented in Figure 8. Above $Z \sim 10^{-2}$, there is an increase in the number of NS-NS mergers and a drop in the number of BH-NS and BH-BH mergers. This is caused by a higher relative frequency of black holes at low metallicity, and a higher relative frequency of neutron stars at high metallicity.

5.3. *Comparison with GCE Studies*

In Figure 10, we compare the normalized numbers of NS-NS mergers extracted from GCE studies (blue) with the numbers predicted by population synthesis models (green). The blue circles have been computed assuming that each NS-NS merger ejects $10^{-5}\,{\rm M}_\odot$ of Eu and that CC SNe eject on average $3.35 \times 10^{-4}\,{\rm M}_\odot$ of Fe per units of stellar mass formed (which is the median value taken from the lower panel of Figure 1). To consider the wide range of Eu and Fe yields and to highlight the possible numbers of NS-NS mergers that can reproduce the same [Eu/Fe] level as the blue circles, we added in Figure 10 in the blue vertical lines. To do so, we considered the lowest and largest Fe yields presented in Figure 1, assumed that the total mass ejected by NS-NS mergers ranges between 0.001 and $0.025\,{\rm M}_\odot$ (see Section 2.1), and used equation (1) to calculate the lower and upper limits. We did not account for the uncertainties in the choice of solar normalization and in the mass fraction of Eu in the solar r-process residual, as they are not significant compared to the uncertainty associated with the total mass ejected by NS-NS mergers. The dark green shaded area represents the range of values predicted by the standard population synthesis model at different metallicities, while the light green shaded area also includes our two alternative models (see Figure 9).

As seen in Figure 10, all GCE studies overlap with the optimistic population synthesis model, and half of them overlap with the standard model as well. But in general, it appears that GCE systematically needs more NS-NS mergers than what is predicted by population synthesis models. We warn that the comparison shown in Figure 10 can be misleading, as $N_{\rm NS-NS}$ is constant in GCE studies while it is metallicity-dependent in population synthesis models.

5.4. *Combining OMEGA and Population Synthesis*

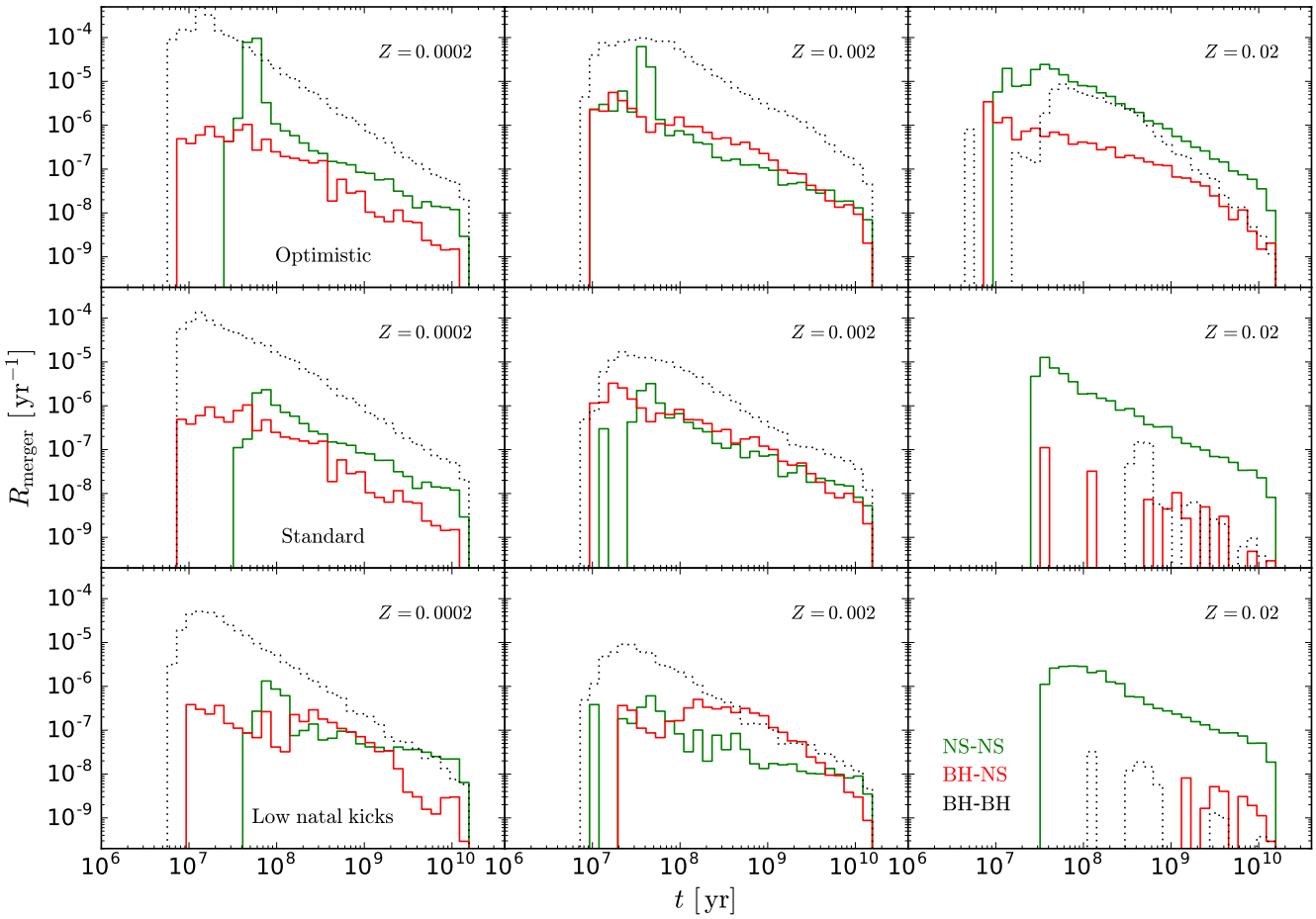

FIG. 8.— NS-NS (green), BH-NS (red), and BH-BH (black) merger rates, as a function of time, predicted by population synthesis models for a stellar population of 2.8×10^8 M$_\odot$. Different columns represent different metallicities, while different rows represent models with different evolutionary assumptions.

To better capture the impact of the metallicity-dependent predictions of population synthesis models in a GCE context, we included them in `OMEGA` as an input parameter. We note that Mennekens & Vanbeveren (2014, 2016) also introduced population synthesis predictions in a GCE code. Figure 11 shows our GCE predictions using NS-NS mergers only (upper panel), BH-NS mergers only (middle panel), and both NS-NS and BH-NS mergers (lower panel). In all cases, the normalization of the DTD functions, or the total number of compact binary mergers, is directly taken from population synthesis predictions. To better visualize the role of compact binary mergers, we switched off the contribution of AGB stars in the evolution of Eu, as they provided a minimum floor value of [Eu/Fe] ~ -1 at high [Fe/H] and prevented us from visualizing the contribution NS-NS and BH-NS mergers.

The solid lines represent the standard model and the dark shaded areas show the range of predictions generated by assuming different ejected masses for the merger events. Alternative models are treated in the same manner and are shown with the dashed lines and the light shaded areas. We assumed that each BH-NS merger event ejects between 10^{-4} and 10^{-1} M$_\odot$ of r-process material (see Section 2.1). We then assumed, as a fiducial case, that only 20 % of all BH-NS mergers are able to eject material. However, we allowed this pourcentage to vary from 2 % to 40 %, representing low and high black hole spins (see Section 2.1.2). This extra source of variation has been combined with the range of total masses ejected by BH-NS mergers in order to generate the shaded areas in Figure 11.

BH-NS mergers appear earlier than NS-NS mergers at low metallicity, which was also seen in Figure 8. We recall that our predictions at [Fe/H] $\lesssim -2$ would be different if we had used a more complex simulation with hydrodynamics or cosmological structure formation (see discussions in Section 4.2). The numerical predictions with BH-NS mergers only (see middle panel of Figure 11) tend to drop near solar metallicity because of the lower frequency of black holes at high metallicity (see references in Section 5.1.3). On the other hand, except for the optimistic DTD functions, our GCE predictions tend to increase near solar metallicity when using NS-NS mergers only (see upper panel of Figure 11), which is caused by a higher frequency of neutron stars. This increasing trend is not consistent with the observed monotonic decreasing trend of [Eu/Fe] at [Fe/H] $\gtrsim -1$.

Our GCE predictions show that it is difficult to explain the current content of Eu in the Milky Way, at

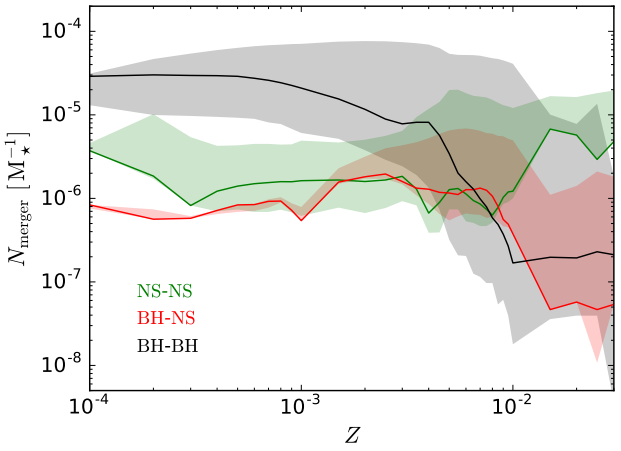

FIG. 9.— Number of NS-NS (green), BH-NS (red), and BH-BH (black) merger, per unit of stellar mass formed as a function of metallicity, predicted by population synthesis models. The solid lines represent the standard model while the shaded areas show the range of possible predictions defined by the two alternative models.

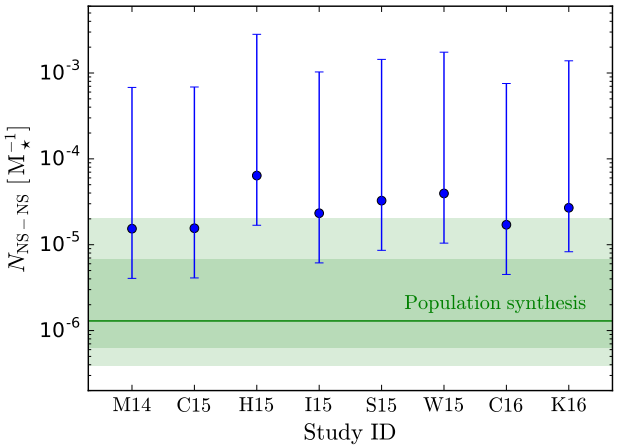

FIG. 10.— Comparison between the normalized number of NS-NS mergers needed in CGE (blue) and the predictions from population synthesis models (green). The solid green line represents the median value of the standard model, using equally spaced metallicities. The dark green shaded area shows the range of values predicted by the standard model at different metallicities, while the light shaded area shows the same range once the two alternative models are included. The blue circles represent the normalized values obtained using the fiducial ejected mass of Eu ($10^{-5}\,M_\odot$) per NS-NS merger event and the median ejected mass of Fe ($3.35\times10^{-4}\,M_\odot$) per stellar mass formed (see Figure 1). The blue vertical lines highlight the range of values that can predict the same level of [Eu/Fe] than the blue circles, which is defined by the plausible range of total masses ejected by NS-NS mergers (see Section 2.1.1) and by the variety of massive star Fe yields adopted in different GCE studies (see Figure 1).

[Fe/H] $\sim$ 0, using the relatively low merger frequencies predicted by population synthesis models. This discrepancy is caused by the normalization of the predicted DTD functions rather than by the shape of those functions, as shown in Figure 10. We note that our predicted [Eu/Fe] ratios could be enhanced by a factor of ~ 5 if we had used the less iron-rich yield setup of other GCE studies (see lower panel of Figure 1). Therefore we conclude that the GCE requirement and population synthesis predictions can be in agreement, but only with the most optimistic merger rates, the largest Eu yields, and the lowest Fe yields.

6. COMPARISON WITH ADVANCED LIGO

As mentioned in the previous sections, the total number of NS-NS mergers needed in GCE studies over a broad range of approaches are all consistent within a factor of ~ 4. This quantity, convolved with the cosmic star formation history, can be converted into a cosmic NS-NS merger rate that can directly be compared with the current and upcoming Advanced LIGO measurements.

6.1. *Cosmic Star Formation History*

The cosmic star formation rate (CSFR) formula, as a function of redshift (z), has been taken from the recent study of Madau & Dickinson (2014),

$$\mathrm{SFR}(z) = 0.015\,\frac{(1+z)^{2.7}}{1+[(1+z)/2.9]^{5.6}} \quad [\mathrm{M_\odot\,Mpc^{-3}\,yr^{-1}}]. \quad (2)$$

Due to the reddening and scarcity of good observational constraints, the CSFR is not well established at $z > 2$. The adopted formula is therefore very likely to represent a lower limit of the actual CSFR at such high redshifts. The adopted model does not fully correct for the small galaxies that were not measured in UV surveys, cannot account for the reionization of the Universe at high-redshift, and underpredicts the observed gamma ray burst rate (Kistler et al. 2009; Horiuchi et al. 2011; Mitchell-Wynne et al. 2015). Increasing the CSFR would increase the rate of double compact object mergers. However, it is not clear to which extent the CSFR should be increased. The adopted CSFR can be seen in Figure 1 of Belczynski et al. (2016c).

6.2. *Convolution Process*

To translate the NS-NS merger implementations found in GCE studies into cosmic NS-NS merger rate densities, the CSFR is used as if it was the input star formation history of a simple GCE model. At each step (redshift bin), a *stellar population* is formed with a specific mass in units of $\mathrm{M_\odot\,Gpc^{-3}}$. For each one of them, the evolution of the NMS rate is defined by the DTD function and its normalization. At any redshift, the overall merger rate density is then obtained by summing the contribution of all *stellar populations*, which all have different ages.

On the other hand, because our population synthesis models are metallicity dependent, the convolution process into a cosmic framework necessitates an extra step. The properties of compact binary objects first need to be obtained as a function of redshift (see Belczynski et al. 2016a). To do so, we assume that the evolution of the mean metallicity as a function of redshift is given by the following formula, which is a modified version of the one found in Madau & Dickinson (2014),

$$\log\left(Z_{\rm mean}(z)\right) = 0.5 + \log\left(\frac{y\,(1-R)}{\rho_{\rm b}}\int_z^{20}\frac{97.8\times10^{10}\,\mathrm{SFR}(z')}{H_0\,E(z')\,(1+z')}dz'\right). \quad (3)$$

In this last equation, the fraction of the stellar mass

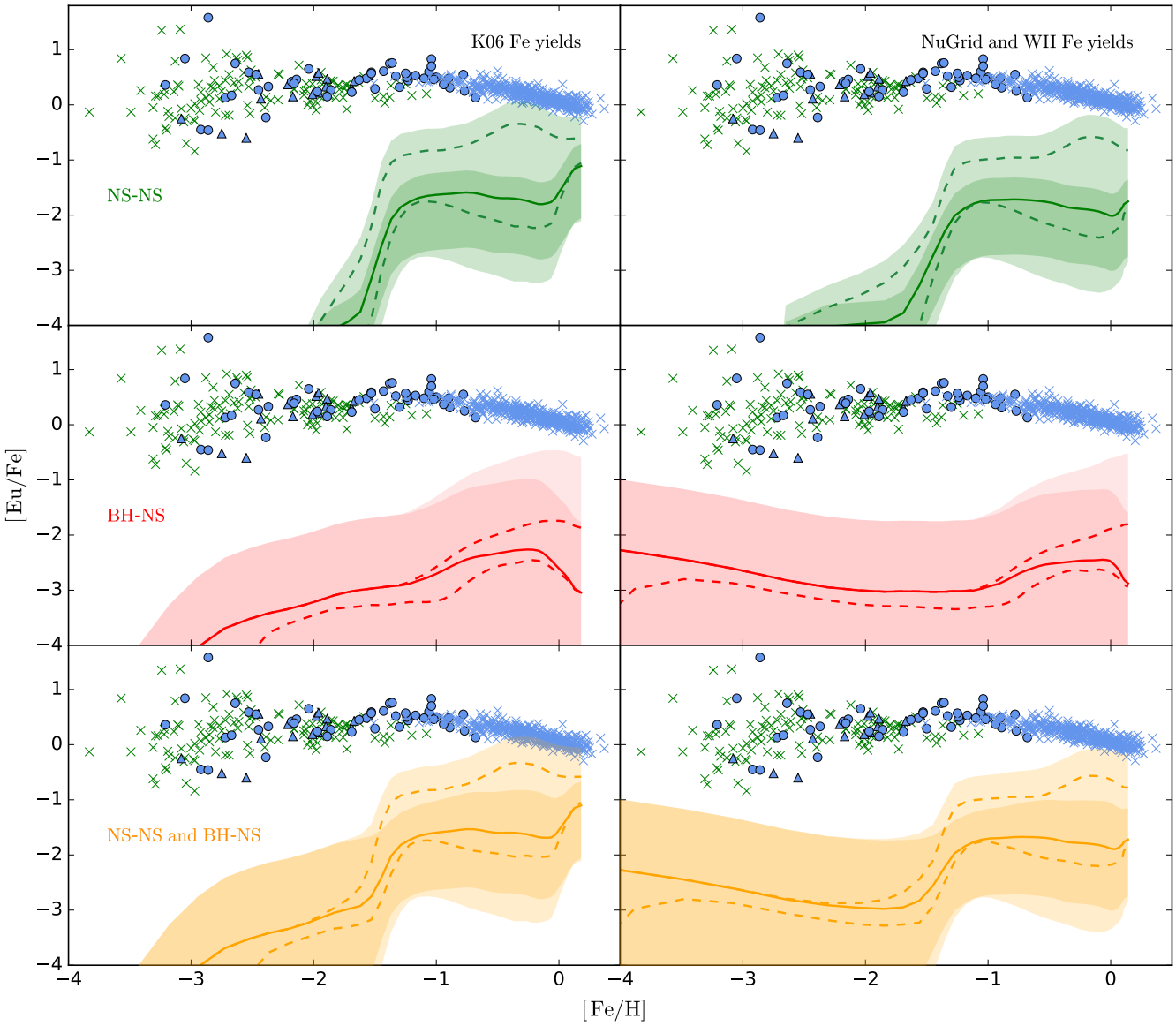

FIG. 11.— Predicted chemical evolution of Eu using the metallicity-dependent population synthesis predictions of compact binary merger rates, combined with the Fe yields calculated by Kobayashi et al. (2006, left panels) and by West & Heger (in preparation) and NuGrid (right panels). The upper, middle, and lower panels represent, respectively, the cases with NS-NS mergers only, with BH-NS mergers only, and with both NS-NS and BH-NS mergers. We note that our IMF and yields setup typically generates more Fe than in other studies (see Figure 1). Using alternative setups could then increase our predicted [Eu/Fe] levels by a factor of ~ 5. The solid lines represent the standard population synthesis models while the dashed lines represent the alternative models. The dark and light shaded areas show the possible predictions defined by the wide range of masses ejected by NS-NS and by BH-NS mergers, for the standard model and the alternative models, respectively. The observational data are the same as in Figure 6.

ejected and returned into the interstellar medium is $R = 0.27$, the net metal yields of stellar ejecta is $y = 0.019$, the baryon density is given by

$$\rho_{\rm b} = 2.77 \times 10^{11}\,\Omega_{\rm b}\,h_0^2\,{\rm M}_\odot\,{\rm Mpc}^{-3}, \qquad (4)$$

the CSFR is taken from equation (2), and

$$E(z) = \sqrt{\Omega_{\rm M}(1+z)^3 + \Omega_{\rm k}(1+z)^2 + \Omega_\Lambda}. \qquad (5)$$

The selected cosmological parameters are $\Omega_{\rm b} = 0.045$, $\Omega_\Lambda = 0.7$, $\Omega_{\rm M} = 0.3$, $\Omega_{\rm k} = 0$, $h_0 = 0.7$, and $H_0 = 70\,{\rm km\,s^{-1}\,Mpc^{-1}}$.

We have increased the mean level of metallicity by 0.5 dex at each redshift to be in a better agreement with observational data (Vangioni et al. 2015). At each redshift, we assume a log-normal distribution of metallicity around the mean value with a dispersion of 0.5 dex (see Dvorkin et al. 2015). This metallicity evolution is presented in the Figure S2 of the supplementary material of Belczynski et al. (2016b). We note that Vangioni et al. (2016) used the cosmic star formation history along with population synthesis models to provide predictions for the evolution of r-process elements.

6.3. *Predicted Cosmic Merger Rates*

Figure 12 shows the cosmic NS-NS merger merger rates predicted by population synthesis models (green) and

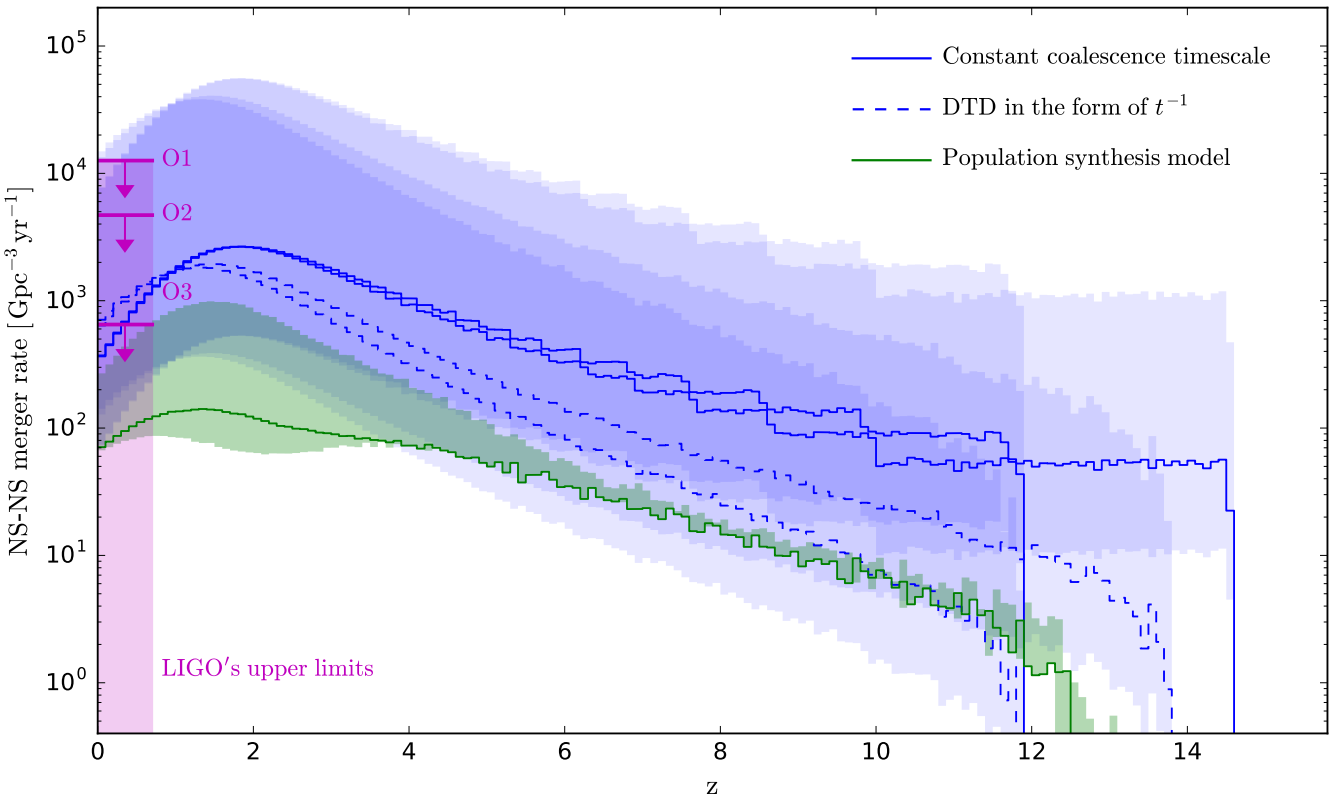

FIG. 12.— Predicted cosmic NS-NS merger rate densities as a function of redshift. The blue lines show the rate needed in galactic chemical evolution simulations, assuming different delay-time distribution functions (different line styles) and a total of 2×10^{-5} NS-NS merger event per stellar mass formed. The blue shaded areas highlight the possible range of values generated by using different ejected masses for NS-NS mergers and different Fe yields for massive stars (see Figure 10). The green line shows the predictions associated with the standard population synthesis model, while the green shaded area shows the possible range of values defined by the two alternative models. The pink shaded area represents the upper limits established by Advanced LIGO during their first run of observations (Abbott et al. 2016b). O1 shows the current established value, while O2 and O3 are the expected values for the next observing runs. The Advanced LIGO horizon goes up to $z \sim 0.7$ for the most massive BH-BH mergers, but should be reduced for NS-NS and BH-NS mergers.

needed by GCE studies to reproduce the stellar abundances of Eu (blue). The green shaded area represents the range of rates defined by the alternative population synthesis models. For the GCE studies, we assumed a total number of NS-NS mergers per stellar mass formed of 2×10^{-5}, a coalescence timescales of 10 and 100 Myr (solid blue lines), as in M14, C15, H15, I15, W15, and Section 4.1, and a DTD function in the form of t^{-1} (dashed blue lines) from 30 and 100 Myr to 10 Gyr, as in S15, van de Voort et al. 2015, K16, and Section 4.2. The blue shaded areas represent the range of rates that can produce the same level of [Eu/Fe], which is defined by considering the possible range of values for the total mass ejected by NS-NS mergers and the mass of Fe ejected by massive stars (see blue lines in Figure 10). We note that the NS-NS frequency adopted to calculate the predictions inferred by GCE studies (blue lines in Figure 12) is actually lower than what is needed in most GCE studies (see blue circles in Figure 10). The pink lines show the current (O1) and expected (O2, O3) upper limits established by Advanced LIGO during their first run of observations (Abbott et al. 2016b). Predictions derived from population synthesis models are well below the O3 upper limit, while the ones derived from GCE studies overlap with all upper limits. Choosing between a constant coalescence timescale or a power law for the DTD function of NS-NS mergers in GCE studies only changes the final cosmic merger rates by a factor of two at most.

Using Figure 12 as a reference, upcoming LIGO measurements will provide a constraint for both population synthesis models and GCE studies. They will help to define whether or not NS-NS mergers can be the main source of r-process elements in the Milky Way and its satellite galaxies. If the measured cosmic NS-NS merger rate, or its upper limit, drops below what is required in GCE studies when assuming NS-NS mergers are the exclusive production sites of r-process elements, additional sites such as CC SNe are necessary (but see Section 7). In order to benefit from upcoming Advanced LIGO measurements and to better quantify the contribution of NS-NS mergers, the range of predictions associated with GCE studies (blue shaded areas in Figure 12) needs to be reduced. We note that the thickness of the green shaded area associated with population synthesis models should be considered as a lower limit, as a complete study of plausible binary evolutionary scenarios still needs to be conducted (see Section 5.1.4).

The main assumption behind Figure 12 is that the GCE requirement extracted from Milky Way models and simulations is universal and representative of all galaxies that hosted the NS-NS mergers that *will* be visible

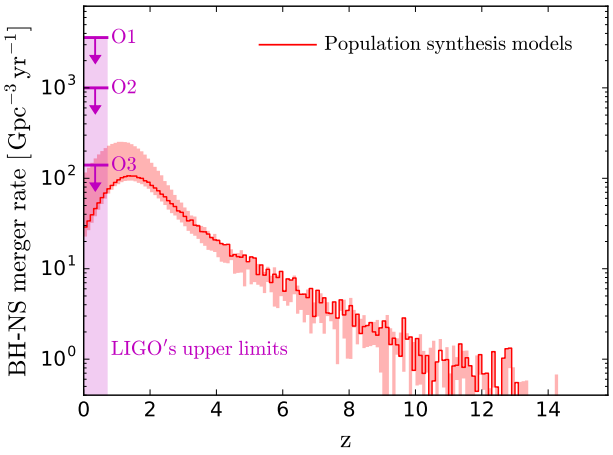

FIG. 13.— Cosmic BH-NS merger rate as a function of redshift predicted by population synthesis models. The lines and shaded areas are similar to the ones found in Figure 12.

inside the LIGO horizon (up to $z \sim 0.1$). For completeness, we show in Figure 13 the analogous of Figure 12 but for BH-NS mergers for population synthesis models. As for NS-NS mergers, the predicted cosmic BH-NS merger rates are well below the O3 measured upper limit.

7. DISCUSSION

In this section, we highlight additional sources of uncertainty that can affect our conclusions and discuss the contribution of CC SNe on the production of r-process elements.

7.1. *Type Ia Supernovae*

SNe Ia are believed to be significant sources of Fe in the Milky Way (e.g., Matteucci et al. 1986; François et al. 2004; Kobayashi et al. 2015). However, different GCE studies can adopt different SN Ia implementations in terms of Fe yields (e.g., Thielemann et al. 1986; Iwamoto et al. 1999; Travaglio et al. 2004; Seitenzahl et al. 2013), total number of explosions (e.g., Maoz et al. 2014; Côté et al. 2016a), and delay-time distribution functions (e.g., Matteucci & Recchi 2001; Matteucci et al. 2009; Yates et al. 2013). Those differences, especially for the yields and total number of explosion, represent another source of uncertainty that can affect the derived number of NS-NS mergers needed to reproduce the observed [Eu/Fe] vs [Fe/H] relationship. Considering a correction for SNe Ia could improve the normalization process presented in Section 3.9 and shown in Figure 5.

7.2. *Galactic Outflows*

A significant source of uncertainty in modeling the early evolution of a galaxy is the fraction of metals that is retained inside galaxies. From a cosmological structure formation point of view, the high-redshift Universe should be mainly composed of low-mass building block galaxies. This implies that galactic outflows should have been more important in the past, as dwarf galaxies are believed to have stronger and more metal-rich outflows than more massive systems (e.g., Tremonti et al. 2004; Peeples & Shankar 2011; Hopkins et al. 2012; Shen et al. 2012; Muratov et al. 2015). Even in the Local Universe, the majority of the metals that had been produced by stars seem to be found outside galaxies (see the COS-Halo survey, Peeples et al. 2014).

Depending on the outflow history and on the production site for r-process elements, Eu and Fe may not be returned into the interstellar medium on the same timescales and therefore might not be retained inside galaxies in the same proportion. On the other hand, the mass ejected from galaxies can also stay bounded to the virialized system and eventually be reintroduced inside galaxies and recycled into stars. Those gas exchanges between galaxies and their circumgalactic medium could impact the chemical evolution of Eu, depending on the different recycling timescales and on the fraction of matter retained inside dark matter halos.

7.3. *Escaping Binaries*

Binary systems receive systemic velocities during the formation of compact remnants both because of the mass lost during the explosions and the kick imparted onto neutron stars and black holes at birth (see Fryer et al. 1998 for a review). Population synthesis models of NS-NS and BH-NS systems show that they have velocities ranging from 50 to 1000 km s^{-1} (Fryer et al. 1999). Because binary systems can sometime be accelerated beyond the escape velocity of their host galaxy, some of the NS-NS and BH-NS mergers should occur outside galaxies (Fryer et al. 1999; Bloom et al. 1999; Belczynski et al. 2006). Observations of short-duration gamma-ray bursts validated this model (Fong & Berger 2013), assuming NS-NS and BH-NS mergers are the progenitors of those bursts. On the other hand, some fraction of compact binary systems have lower proper motions below $\sim$30 km/s (Kramer et al. 2006; Beniamini & Piran 2016). Fryer et al. (1998, 1999) calibrated their NS kick distribution to match the observed features of these low-velocity binary systems while also matching the pulsar velocity distributions and the formation rates of X-ray binaries. This led to a bimodal kick distribution and more low-velocity binaries compared to the single-mode kick distributions assumed in this work (see Section 5).

It is difficult at this point to derive the exact fraction of escape binaries. Systems that received large spatial velocities and escaped their birth sites could be harder to detect, which may induce an observational bias. But if compact binary systems can escape their host galaxies, and are the main source of the r-process, this could imply that a fraction of r-process elements can be found outside galaxies while the Fe ejected by the progenitor stars could still be found inside galaxies. This should induce an uncertainty in the derived number of compact binary mergers needed in order to reproduce the [Eu/Fe] ratios in GCE studies. This phenomena should be more important in the early Universe where galaxies were smaller in size. As a matter of fact, Belczynski et al. (2006) suggested that, for small elliptical galaxies, the majority of compact binary mergers occur outside their host galaxies. We note that massive stars can also be ejected outside galaxies by dynamical interactions such as disruptions of binary systems or close encounters with the galactic center. However, as discussed in Section 7.2, the Eu ejected outside galaxies could still be reintroduced inside galaxies after a certain time, depending on the dark matter gravitational potential well of the host galaxy when es-

caping binary mergers occur.

7.4. *Stellar Remnants*

The stellar remnant mass distribution plays a crucial role in both chemical evolution and population synthesis models, as it determines the relative fraction of black holes and neutron stars. Several observations suggest that the high-mass end of the massive star spectrum should preferentially form black holes – the lack of CC SN progenitor stars with initial mass above $18\,M_\odot$ (Smartt 2015), the black hole mass distribution function (e.g., Belczynski et al. 2012), the failed explosion of a $25\,M_\odot$ star (Adams et al. 2016), and the merger of two black holes of $\sim 30\,M_\odot$(Abbott et al. 2016a). A similar conclusion is motivated by theory (e.g., Fryer 1999; Heger et al. 2003) but can be more complex with predictions of islands of non-explodability (Ugliano et al. 2012; Ertl et al. 2016; Sukhbold et al. 2016) and of highly non-monotonic relations between the stellar initial and final masses resulting from binary interactions (e.g, Belczynski & Taam 2008).

For GCE applications, accounting for direct black hole formation generates different chemical evolution predictions compared to when all massive stars are assumed to produce a CC SN (see Côté et al. 2016b). When stellar yields use a relatively flat and low remnant mass distribution (e.g., K06; Chieffi & Limongi 2013), the ejected masses of alpha and iron-peak elements stay roughly constant or continuously increase as a function of stellar initial mass. When using stellar yields that account for black hole formation (e.g., Fryer et al. 2012; Pignatari et al. 2016; C. Ritter et al. in preparation), the ejected mass for all metals usually start to decrease in stars more massive than $\sim 25\,M_\odot$.

Depending on the set of yields and the adopted remnant mass distribution, predictions for the evolution of alpha and iron-peak elements, including Fe, can significantly differ and can thus modify the number of NS-NS and BH-NS mergers needed in GCE studies to reproduce the observed [Eu/Fe] abundance ratios. In addition varying the remnant mass distribution in stellar populations can also modify the overall rates of NS-NS and BH-NS mergers. Because these two types of binary mergers do not necessarily produce the same ejecta (see Section 2.1), the choice of the remnant mass distribution can therefore have an impact on the total mass of r-process elements returned into the interstellar medium and recycled into stars.

7.5. *Core-Collapse Supernovae*

In this paper, compact binary mergers have been considered as the exclusive production sites of r-process elements, as our goal was to investigate whether or not NS-NS mergers alone can reproduce the current amount of Eu observed in the stars of the Milky Way. The relative contribution, especially at low [Fe/H], of NS-NS mergers is still highly debated and CC SNe could still be important production sites. M14 suggested an early enrichment by CC SNe originating from progenitor stars in the mass range of $12-30\,M_\odot$, $20-50\,M_\odot$, or a combination of these, which is also suggested by C15. Another production site of r-process elements are the magnetorotationally driven SNe (MHD SNe, e.g., Winteler et al. 2012; Nishimura et al. 2015). These rare SNe generate highly magnetized and fast rotating neutron stars that represent $\lesssim 1\,\%$ of all neutron stars. C15 and W15 adopted a combined environment which considers the contributions of both NS-NS mergers and MHD SNe as r-process production sites and found that such combinations are able to explain the observed r-process abundances, especially at low [Fe/H].

Although we only considered compact binary mergers in our study, it should be noted that other production sites can still contribute significantly to the evolution of the r process. Our appellation of *how many NS-NS mergers are needed in GCE studies* should be considered as an upper limit of the actual contribution of such events.

8. SUMMARY AND CONCLUSIONS

A connection between GCE, population synthesis models, and Advanced LIGO measurements have been made in order to investigate whether or not NS-NS mergers (and compact binary mergers in general) can be the main source of r-process elements in the Milky Way. We have compiled and reviewed eight GCE studies, including our own, and extracted how many NS-NS mergers are needed in order to reproduce the evolution of Eu in our Galaxy. Those studies include a wide rage of numerical setup from simple one-zone homogeneous-mixing models to cosmological hydrodynamic simulations. In spite of the different levels of complexity of the considered studies, we found that, once normalized, the needed number of NS-NS mergers converges within a factor of ~ 4 (but see Section 7).

Using `OMEGA`, our one-zone GCE code, we explored the impact of using different DTD functions for NS-NS mergers on our ability to reproduce the Eu abundances trend. Using a constant coalescence timescale, after which all NS-NS mergers occur in a simple stellar population, our predictions regarding the evolution of Eu are consistent with previous studies that used a similar implementation. We cannot reproduce, however, observations at low [Fe/H] when using long-lasting DTD functions in the form of a power law with an index of -1 or lower. This highlights the inability of simple models to capture the early evolution of our Galaxy, as more complex simulations that include hydrodynamics (S15; H15; van de Voort et al. 2015) and a proper treatment of cosmological structure formation (K16) can reproduce, using NS-NS mergers only, the Eu abundances of metal-poor halo stars, even with long-lasting DTD functions. Nevertheless, the overall number of NS-NS mergers needed to reach [Eu/Fe] ~ 0 at [Fe/H] ~ 0 is relatively insensitive of the choice of the DTD function.

We compared the number of NS-NS mergers needed in GCE studies with the predictions of population synthesis models, accounting for the wide range of total masses ejected by NS-NS mergers and Fe yields associated with massive stars. We then introduced the metallicity-dependent NS-NS and BH-NS mergers rates predicted by population synthesis models into our GCE model as an input to see their impact in a GCE context. Finally, we convolved the GCE needed NS-NS merger implementations and population synthesis predictions with the cosmic star formation history to provide results that can directly be compared with upcoming Advanced LIGO measurements. Our main conclusions are

the following:

- GCE typically requires about 10 times more NS-NS mergers than what is predicted by our standard population synthesis models, when assuming that the ejected r-process mass is $0.01\,M_\odot$ per merger event.
- It is difficult to reproduce Eu observations by introducing the metallicity-dependent populations synthesis predicted rates into our GCE model, even when considering both NS-NS and BH-NS mergers.
- GCE and population synthesis can only be in agreement when assuming optimistic rates, high Eu yields, and low Fe yields.
- The cosmic NS-NS and BH-NS merger rate densities predicted using population synthesis models are below all upper limits currently established by Advanced LIGO. The cosmic NS-NS merger rate densities inferred using the GCE requirement are uncertain by a factor of ~ 150 and overlap with all upper limits.
- Our population synthesis models suggest that BH-NS mergers appear earlier (at lower [Fe/H]) than NS-NS mergers but overall, contribute less to the evolution of the r process. This is under the assumption that the maximum ejected mass is $0.1\,M_\odot$ per merger event and that no more than half of BH-NS mergers can eject material (see Section 2.1.2).

At the moment, population synthesis models and GCE studies are in agreement with the O1 upper limit currently established by Advanced LIGO. Using Figure 12 as a future reference, Upcoming Advanced LIGO measurements will provide valuable insights on the plausibility of the GCE requirement and will help to define whether or not NS-NS mergers can be the main source of the r-process elements. We recall that our conclusions are based on the assumption that NS-NS mergers should not, on average, eject more than $0.025\,M_\odot$ of material per merger event (see Section 2.1.1). Furthermore, we recall that our alternative population synthesis models may not be representative of the complete plausible range of NS-NS and BH-NS merger rates. More calculations are needed in order to isolate extreme cases that will provide more realistic evolutionary uncertainties.

Besides the detection of gravitational waves that can constrain the rate of compact binary mergers, kilonovae could constrain the mass ejected by NS-NS mergers. However, current uncertainties in the opacities (Fontes et al. 2015) make it difficult to extract the r-process ejecta from a kilonova observation. Both detailed observations and high-fidelity models are needed. But if they can be done, these detections could be use to constrain the r-process ejected mass.

Many sources of uncertainty, such as the yields ejected by compact binary mergers, the binary escape fraction, the circulation of gas inside and outside galaxies, the cosmic star formation history, and different SN Ia implementations, can still affect the reliability of our conclusions. Ongoing work in nuclear astrophysics, in observation, and in galaxy evolution will hopefully contribute to reduce the current level of uncertainty, which will lead to a better quantification of the role played by compact binary mergers in the evolution of r-process elements.

ACKNOWLEDGEMENTS

We are thankful to Yutaka Hirai and Yutaka Komiya for sharing details of their chemical evolution codes, to Marco Pignatari for providing useful analysis on NuGrid stellar models, to Christopher West and Alexander Heger for providing unpublished stellar yields, and to Oleg Korobkin for discussions on the r process. This research is supported by the National Science Foundation (USA) under Grant No. PHY-1430152 (JINA Center for the Evolution of the Elements), and by the FRQNT (Quebec, Canada) postdoctoral fellowship program. KB acknowledges support from the NCN grants Sonata Bis 2 (DEC-2012/07/E/ST9/01360), OPUS (2015/19/B/ST9/01099) and OPUS (2015/19/B/ST9/03188). CLF is funded in part under the auspices of the U.S. Department of Energy, and supported by its contract W-7405-ENG-36 to Los Alamos National Laboratory. BW is supported by the European Research Council (FP7) under ERC Advanced Grant Agreement No. 321263 - FISH, and the Swiss National Science Foundation (SNF). The Basel group is a member in the COST Action New CompStar. BWO was supported by the National Aeronautics and Space Administration (USA) through grant NNX12AC98G and Hubble Theory Grant HST-AR-13261.01-A.

REFERENCES

Aasi, J., Abbott, B. P., Abbott, R., & the LIGO Scientific Collaboration 2015, CQGra, 32, 4001
Abadie, J., Abbott, B. P., Abbott, R., et al. 2010, ApJ, 715, 1453
Abbott, B. P., Abbott, R., Abbott, T. D., et al. 2016a, PhRvD, 93, 122003
Abbott, B. P., Abbott, R., Abbott, T. D., the LIGO Scientific Collaboration, & the Virgo Collaboration 2016b, arXiv:1607.07456
Abbott, B. P., Abbott, R., Adhikari, R., et al. 2009, RPPh, 72, 6901
Adams, S. M., Kochanek, C. S., Gerke, J. R., Stanek, K. Z., & Dai, X. 2016, arXiv:1609.01283
Arcones, A., & Martínez-Pinedo, G. 2011, PhRvC, 83, 4
Arcones, A., & Thielemann, F.-K. 2013, JPhG, 40, 3201
Argast, D., Samland, M., Thielemann, F.-K., & Qian, Y.-Z. 2004, A&A, 416, 997
Arnould, M., Goriely, S., & Takahashi, K. 2007, PhR, 450, 97
Battistini, C., & Bensby, T. 2015, A&A, 577, 9
Battistini, C., & Bensby, T. 2016, A&A, 586, 49
Bauswein, A., Ardevol Pulpillo, R., Janka, H.-T., & Goriely, S. 2014, ApJ, 795, L9
Bauswein, A., Goriely, S., & Janka, H.-T. 2013, ApJ, 773, 78
Belczynski, K., Bulik, T., Fryer, C. L., Ruiter, A., Valsecchi, F., Vink, J. S., & Hurley, J. R. 2010, ApJ, 714, 1217
Belczynski, K., Heger, A., Gladysz, W., et al. 2016c, arXiv:1607.03116
Belczynski, K., Holz, D. E., Bulik, T., & O'Shaughnessy, R. 2016b, Nature, 534, 512
Belczynski, K., Kalogera, V., & Bulik, T. 2002, ApJ, 572, 407
Belczynski, K., Kalogera, V., Rasio, F. A., Taam, R. E., Zezas, A., Bulik, T., Maccarone, T. J., & Ivanova, N. 2008a, ApJS, 174, 223

Belczynski, K., Perna, R., Bulik, T., Kalogera, V., Ivanova, N., & Lamb, D. Q. 2006, ApJ, 648, 1110
Belczynski, K., Repetto, S., Holz, D. E., O'Shaughnessy, R., Bulik, T., Berti, E., Fryer, C., & Dominik, M. 2016a, ApJ, 819, 108
Belczynski, K., & Taam, R. E. 2008, ApJ, 685, 400
Belczynski, K., Taam, R. E., Kalogera, V., Rasio, F. A., & Bulik, T. 2007, ApJ, 662, 504
Belczynski, K., Taam, R. E., Rantsiou, E., & van der Sluys, M. 2008b, ApJ, 682, 474
Belczynski, K., Wiktorowicz, G., Fryer, C. L., Holz, D. E., & Kalogera, V. 2012, ApJ, 757, 91
Beniamini, P., Hotokezaka, K., & Piran, T. 2016, ApJ, 832, 149
Beniamini, P., & Piran, T. 2016, MNRAS, 456, 4089
Bensby, T., Feltzing, S., & Oey, M. S. 2014, A&A, 562, A71
Berger, E., Fong, W., & Chornock, R. 2013, ApJ, 774, 23
Bloom, J. S., Sigurdsson, S., & Pols, O. R. 1999, MNRAS, 305, 763
Cayrel, R., Depagne, E., Spite, M., et al. 2004, A&A, 416, 1117
Cescutti, G. 2008, A&A, 481, 691
Cescutti, G., Romano, D., Matteucci, F., Chiappini, C., & Hirschi, R. 2015, A&A, 577, 139
Chabrier, G. 2003, PASP, 115, 763
Chiappini, C., Ekstr/"om, S., Meynet, G., Hirschi, R., Maeder, A., & Charbonnel, C. 2008, A&A, 479, 9
Chiappini, C., Matteucci, F., & Gratton, R. 1997, ApJ, 477, 765
Chiappini, C., Matteucci, F., & Romano, D. 2001, ApJ, 554, 1044
Chieffi, A., & Limongi, M. 2013, ApJ, 764, 21
Côté, B., O'Shea, B. W., Ritter, C., Herwig, F., & Venn, K. A. 2016c, arXiv:1604.07824
Côté, B., Ritter, C., Herwig, F., O'Shea, B. W., Pignatari, M., Silvia, D., Jones, S., & Fryer, C. L., 2016d, arXiv:1609.09528
Côté, B., Ritter, C., O'Shea, B. W., Herwig, F., Pignatari, M., Jones, S., & Fryer, C. L. 2016a, ApJ, 824, 82
Côté, B., West, C., Heger, A., Ritter, C., O'Shea, B. W., Herwig, F., Travaglio, C., & Bisterzo, S. 2016b, MNRAS, in press, arXiv:1602.04824
Cohen, J. G., Christlieb, N., Thompson, I., McWilliam, A., Shectman, S., Reimers, D., Wisotzki, L., & Kirby, E. 2013, ApJ, 778, 56
de Mink, S. E., & Belczynski, K. 2015, ApJ, 814, 58
de Mink, S. E., & Mandel, I. 2016, MNRAS, 460, 3545
Dessart, L., Burrows, A., Livne, E., & Ott, C. D. 2007, ApJ, 669, 585
Dominik, M., Belczynski, K., Fryer, C., Holz, D., E., Berti, E., Bulik, T., Mandel, I., & O'Shaughnessy, R. 2012, ApJ, 759, 52
Dvorkin, I., Silk, J., Vangioni, E., Petitjean, P., & Olive, K. A. 2015, MNRAS, 452, L36
Eichler, M., Arcones, A., Käppeli, R., et al. 2016, JPhCS, 665, 2054
Eldridge, J. J., & Stanway, E. R. 2016, MNRAS, 462, 3302
Endrizzi, A., Ciolfi, R., Giacomazzo, B., Kastaun, W., & Kawamura, T. 2016, CQGra, 33, 16
Ertl, T., Janka, T.-H., Woosley, S. E., Sukhbold, T., & Ugliano, M. 2016, ApJ, 818, 124
Fernández, R., & Metzger, B. D. 2013, MNRAS, 435, 502
Fernández, R., Kasen, D., Metzger, B. D., & Quataert, E. 2015, MNRAS, 446, 750
Fong, W., & Berger, E. 2013, ApJ, 776, 18
Fong, W., Margutti, R., Chornock, R., et al. 2016, ApJ, 833, 151
Fontes, C. J., Fryer, C. L., Hungerford, A. L., Hakel, P., Colgan, J., Kilcrease, D. P., & Sherrill, M. E. 2015, High Energy Density Physics, 16, 53
François, P., Matteucci, F., Cayrel, R., Spite, M., Spite, F., & Chiappini, C. 2004, A&A, 421, 613
Fryer, C. L. 1999, ApJ, 522, 413
Fryer, C. L. 2006, New Astron. Rev., 50, 492
Fryer, C. L., Belczynski, K., Ramirez-Ruiz, E., Rosswog, S., Shen, G., & Steiner, A. W. 2015, ApJ, 812, 24
Fryer, C. L., Belczynski, K., Wiktorowicz, G., Dominik, M., Kalogera, V., & Holz, D. E. 2012, ApJ, 749, 91
Fryer, C., Burrows, A., & Benz, W. 1998, ApJ, 496, 333
Fryer, C. L., Woosley, S. E., & Hartmann, D. H. 1999, ApJ, 526, 152
García Pérez, A. E., Allende Prieto, C., Holtzman, J. A., et al. 2016, AJ, 151, 144
Gibson, B. K., Fenner, Y., Renda, A., Kawata, D., & Lee, H.-C. 2003, PASA, 20, 401
Goriely, S. 2015, EPJA, 51, 22
Griffen, B. F., Ji, A. P., Dooley, G. A., Gómez, F. A., Vogelsberger, M., O'Shea, B. W., & Frebel, A. 2016, ApJ, 818, 10
Guedes, J., Callegari, S., Madau, P., & Mayer, L. 2011, ApJ, 742, 76
Hansen, C. J., Primas, F., Hartman, H., Kratz, K.-L., Wanajo, S., Leibundgut, B., Farouqi, K., Hallmann, O., Christlieb, N., & Nilsson, H. 2012, A&A, 545, 31
Heger, A., Fryer, C. L., Woosley, S. E., Langer, N., & Hartmann, D. H. 2003, ApJ, 591, 288
Heger, A., Woosley, S. E. 2010, ApJ, 724, 341
Hirai, Y., Ishimaru, Y., Saitoh, T. R., Fujii, M., Hidaka, J., & Kajino, T. 2015, ApJ, 814, 41
Hobbs, G., Lorimer, D. R., Lyne, A. G., & Kramer, M. 2005, MNRAS, 360, 974
Hopkins, P. F., Quataert, E., & Murray, N. 2012, MNRAS, 421, 3522
Horiuchi, S., Beacom, J. F., Kochanek, C. S., Prieto, J. L., Stanek, K. Z., & Thompson, T. A. 2011, ApJ, 738, 154
Hotokezaka, K., Kiuchi, K., Kyutoku, K., Okawa, H., Sekiguchi, Y., Shibata, M., & Taniguchi, K. 2013a, PhRvD, 87, 2
Hotokezaka, K., Kyutoku, K., Tanaka, M., Kiuchi, K., Sekiguchi, Y., Shibata, M., & Wanajo, S. 2013b, ApJ, 778L, 16
Hotokezaka, K., Piran, T., & Paul, M. 2015, Nature Physics, 11, 1042
Hurley, J. R., Pols, O. R., & Tout, C. A. 2000, MNRAS, 315, 543
Ishimaru, Y., & Wanajo, S. 1999, ApJ, 511, L33
Ishimaru, Y., Wanajo, S., Aoki, W., & Ryan, S. G. 2004, ApJ, 600, L47
Ishimaru, Y., Wanajo, S., & Prantzos, N. 2015, ApJ, 804, 35
Iwamoto, K., Brachwitz, F., Nomoto, K., Kishimoto, N., Umeda, H., Hix, W. R., Thielemann, F.-K. 1999, ApJS, 125, 439
Jin, Z.-P., Li, X., Cano, Z., Covino, S., Fan, Y.-Z., & Wei, D.-M. 2015, ApJ, 811L, 22
Just, O., Bauswein, A., Pulpillo, R. A., Goriely, S., & Janka, H.-T. 2015, MNRAS, 448, 541
Karakas, A. I. 2010, MNRAS, 403, 1413
Kawaguchi, K., Kyutoku, K., Nakano, H., Okawa, H., Shibata, M., & Taniguchi, K. PhRvD, 92, 2
Kistler, M. D., Yüksel, H., Beacom, J. F., Hopkins, A. M., & Wyithe, J. S. B. 2009, ApJ, 705, L104
Kobayashi, C., & Nakasato, N. 2011, ApJ, 729, 16
Kobayashi, C., Nomoto, K., & Hachisu, I. 2015, ApJ, 804, 24
Kobayashi, C., Umeda, H., Nomoto, K., Tominaga, N., & Ohkubo, T. 2006, ApJ, 653, 1145
Kobulnicky, H. A., Kiminki, D. C., Lundquist, M. J., et al. 2014, ApJS, 213, 34
Komiya, Y., & Shigeyama, T. 2016, arXiv:1608.01772
Komiya, Y., Yamada, S., Suda, T., & Fujimoto, M. Y. 2014, ApJ, 783, 132
Korobkin, O., Rosswog. S., Arcones, A., & Winteler, C. 2012, MNRAS, 426, 1940
Kramer, M., Stairs, I. H., Manchester, R. N., et al. 2006, Science, 314, 97
Kroupa, P., Tout, C. A., & Gilmore, G. 1993, MNRAS, 262, 545
Kubryk, M., Prantzos, N., & Athanassoula, E. 2015, A&A, 580, 126
Lehner, N., & Howk, J. C. 2011, Science, 334, 955
Leroy, A. K., Walter, F., Brinks, E., Bigiel, F., de Blok, W. J. G., Madore, B., & Thornley, M. D. 2008, ApJ, 136, 2782
Limongi, M., & Chieffi, A. 2006, ApJ, 647, 483
Lippuner, J., & Roberts, L. F. 2015, ApJ, 815, 82
Macias, P., & Ramirez-Ruiz, E. 2016, arXiv:1609.04826
Macleod, M., & Ramirez-Ruiz, E. 2015, ApJ, 803, 41
Madau, P., & Dickinson, M. 2014, ARA&A, 52, 415
Maoz, D., Mannucci, F., & Nelemans, G. 2014, ARA&A, 52, 107
Marchant, P., Langer, N., Podsiadlowski, P., Tauris, T. M., & Moriya, T. J. 2016, A&A, 588, A50
Martin, C. L. 1999, ApJ, 513, 156
Martin, D., Arcones, A., Nazarewicz, W., & Olsen, E. 2016, PhRvL, 116, 12
Martin, D., Perego, A., Arcones, A., Thielemann, F.-K., Korobkin, O., & Rosswog, S. 2015, ApJ, 813, 2
Matteucci, F. 2014, The Origin of the Galaxy and Local Group, Saas-Fee Advanced Course, 37, 145
Matteucci, F., & Greggio, L. 1986, A&A, 154, 279
Matteucci, F., & Recchi, S. 2001, ApJ, 558, 351
Matteucci, F., Romano, D., Arcones, A., Korobkin, O., & Rosswog, S. 2014, MNRAS, 438, 2177
Matteucci, F., Spitoni, E., Recchi, S., & Valiante, R. 2009, A&A, 501, 531
Mennekens, N., & Vanbeveren, D. 2014, A&A, 564, 134
Mennekens, N., & Vanbeveren, D. 2016, A&A, 589, 64
Minchev, I., Chiappini, C., & Martig, M. 2013, A&A, 558, 9
Minchev, I., Chiappini, C., & Martig, M. 2014, A&A, 572, 92
Mitchell-Wynne, K., Cooray, A., Gong, Y., et al. 2015, Nature Communications, 6, 7945
Mollá, M., Cavichia, O., Gavilán, M., & Gibson, B. K. 2015, MNRAS, 451, 3693
Mumpower, M. R., Surman, R., McLaughlin, G. C., & Aprahamian, A. 2016, PrPNP, 86, 86
Moratov, A. L., Kereš, D., Faucher-Giguère, C.-A., Hopkins, P. F., Quataert, E., & Murray, N. 2015, MNRAS, 454, 2691
Nakamura, K., Kajino, T., Mathews, G. J., Sato, S., & Harikae, S. 2015, A&A, 582, 34

Nishimura, N., Takiwaki, T., & Thielemann, F.-K. 2015, ApJ, 810, 109
Nomoto, K., Hashimoto, M., Tsujimoto, T., Thielemann, F.-K., Kishimoto, N., Kubo, Y., & Nakasato, N. 1997, NuPhA, 616, 79
Nomoto, K., Kobayashi, C., & Tominaga, N. 2013, ARA&A, 51, 457
Pavlovskii, K., Ivanova, N., Belczynski, K., & Van, K. X. 2016, arXiv:1606.04921
Peeples, M. S., & Shankar, F. 2011, MNRAS, 417, 2962
Peeples, M. S., Werk, J. K., Tumlinson, J., Oppenheimer, B. D., Prochaska, J. X., Katz, N., & Weinberg, D. H. 2014, ApJ, 786, 54
Perego, A., Rosswog, S., Cabezón, R. M., Korobkin, O., Käppeli, R., Arcones, A., & Liebendörfer, M. 2014, MNRAS, 443, 3134
Peters, P. C. 1964, Phys. Rev. 136, 1224
Pignatari, M., Herwig, F., Hirschi, R., et al. 2016, ApJS, 225, 24
Podsiadlowski, P., Joss, P. C., & Hsu, J. J. L. 1992, ApJ, 391, 246
Poelarends, A. J. T., Herwig, F., Langer, N., & Heger, A. 2008, ApJ, 675, 614
Radice, D., Galeazzi, F., Lippuner, J., Roberts, L. F., Ott, C., & Rezzolla, L. 2016, MNRAS, 460, 3255
Raiteri, C. M., Villata, M., & Navarro, J. F. 1996, A&A, 315, 105
Ricker, P. M., & Taam, R. E. 2008, ApJ, 672, L41
Roberts, L. F., Lippuner, J., Duez, M. D., Faber, J. A., Foucart, F., Lombardi, J. C. Jr., Ning, S., Ott, C. D., & Ponce, M. 2016, arXiv:1601.07942
Roederer, I. U., Kratz, K.-L., Frebel, A., Christlieb, N., Pfeiffer, B., Cowan, J. J., & Sneden, C. 2009, ApJ, 698, 1963
Roederer, I. U., Preston, G. W., Thompson, I. B., Shectman, S. A., Sneden, C., Burley, G. S., & Kelson, D. D. 2014, AJ, 147, 136
Romano, D., Karakas, A. I., Tosi, M., & Matteucci, F. 2010, A&A, 522, 32
Rosswog, S., Korobkin, O., Arcones, A., Thielemann, F.-K., & Piran, T. 2014, MNRAS, 439, 744
Saitoh, T. R., Daisaka, H., Kokubo, E., Makino, J., Okamoto, T., Tomisaka, K., Wada, K., & Yoshida, N. 2008, PASJ, 60, 667
Saitoh, T. R., Daisaka, H., Kokubo, E., Makino, J., Okamoto, T., Tomisaka, K., Wada, K., & Yoshida, N. 2009, PASJ, 61, 481
Salpeter, E. E. 1955, ApJ, 121, 161
Sana, H., de Mink, S. E., de Koter, A., et al. 2012, Science, 337, 444
Scalo, J. M. 1986, Fundam. Cosm. Phys., 11, 1
Schaye, J., Crain, R. A., Bower, R. G., et al. 2015, MNRAS, 446, 521
Seitenzahl, I. R., Ciaraldi-Schoolmann, F., Röpke, F. K., Fink, M., Hillebrandt, W., Kromer, M., Pakmor, R., Ruiter, A. J., Sim, S. A., & Taubengerger, S. 2013, MNRAS, 429, 1156
Sekiguchi, Y., Kiuchi, K., Kyutoku, K., & Shibata, M. 2015, PhRvD, 91, 6
Sekiguchi, Y., Kiuchi, K., Kyutoku, K., Shibata, M., & Taniguchi, K. 2016, PhRvD, 93, 12
Smartt, S. J. 2015, PASA, 32, 16
Shen, S., Cooke, R. J., Ramirez-Ruiz, E., Madau, P., Mayer, L., & Guedes, J. 2015, ApJ, 807, 115
Shen, S., Madau, P., Aguirre, A., et al. 2012, ApJ, 760, 50
Sneden, C., Cowan, J. J., & Gallino, R. 2008, ARA&A, 46, 241
Stinson, G., Seth, A., Katz, N., Wadsley, J., Governato, F., & Quinn, T. 2006, MNRAS, 373, 1074
Sukhbold, T., Ertl, T., Woosley, S. E., Brown, J. M., & Janka, H.-T.
Tanvir, N. R., Levan, A. J., Fruchter, A. S., Hjorth, J., Hounsell, R. A., Wiersema, K., & Tunniclife, R. L. 2013, Nature, 500, 547
Thielemann, F.-K., Arcones, A., Käppeli, R., et al. 2011, PrPNP, 66, 346
Thielemann, F.-K., Nomoto, K., & Hashimoto, M.-A. 1996, ApJ, 460, 408
Thielemann, F.-K., Nomoto, K., & Yokoi, K. 1986, A&A, 158, 17
Travaglio, C., Hillebrandt, W., Reinecke, M., & Thielemann, F.-K. 2004, A&A, 425, 1029
Tremonti, C. A., Heckman, T. M., Kauffmann, G., et al. 2004, ApJ, 613, 898
Ugliano, M., Janka, H.-T., Marek, A., & Arcones, A. 2012, ApJ, 757, 69
van de Voort, F., Quataert, E., Hopkins, P. F., Kereš, D., & Faucher-Giguère, C.-A. 2015, MNRAS, 447 140
Vangioni, E., Goriely, S., Daigne, F., François, P., & Belczynski, K. 2016, MNRAS, 455, 17
Vangioni, E., Olive, K. A., Prestegard, T., Silk, J., Petitjean, P., & Mandic, V. 2015, MNRAS, 447, 2575
Vink, J. S. 2011, Ap&SS, 336, 163
Vogelsberger, M., Genel, S., Springel, V., Torrey, P., Sijacki, D., Xu, D., Snyder, G., Nelson, D., & Hernquist, L. 2014, MNRAS, 444, 1518
Wanajo, S., & Ishimaru, Y. 2006, NuPhA, 77, 676
Wehmeyer, B., Pignatari, M., & Thielemann, F.-K. 2015, MNRAS, 452, 1970
Weidemann, V. 1987, A&A, 188, 74
Winteler, C., Käppeli, R., Perego, A., Arcones, A., Vasser, N., Nishimura, N., Liebendörfer, M., & Thielemann, F.-K. 2012, ApJ, 750, L22
Woosley, S. E. 2016, ApJ, 824, L10
Woosley, S. E., Heger, A., & Weaver, T. A. 2002, Reviews of Modern Physics, 74, 1015
Woosley, S. E., & Weaver, T. A. 1995, ApJS, 101, 181
Wu, M.-R., Fernández, R., Martínez-Pinedo, G., & Metzger, B. D. 2016, MNRAS, 463, 2323
Yang, B., Jin, Z.-P., Li, X., Convino, S., Zheng, X.-Z., Hotokezaka, K., Fan, Y.-Z., Piran, T., & Wei, D.-M. 2015, NatCo, 6, 7323
Yates, R. M., Henriques, B., Thomas, P. A., Kauffmann, G., Johansson, J., & White, S. D. M. 2013, MNRAS, 435, 3500
Young, P. A., Ellinger, C. I., Arnett, D., Fryer, C. L., & Rockefeller, G. 2009, ApJ, 699, 938

APPENDIX

HIGHLY ECCENTRIC BINARIES

We used a dynamics code to model the periastron distances of compact binary systems for a range of impact parameters and velocities. As an example, for two $1.4\,M_\odot$ neutron stars interacting with an impact velocity of $10\,km\,s^{-1}$, the system remains bound if the impact parameter is 10^{14} cm. But for such wide separations, the resulting periastron is above 10^8 km (see Figure 14). Only when the impact parameter is below 10^{11} cm does the periastron distance drops below 20 km, which would allow NS-NS mergers to eject more than $0.025\,M_\odot$ of r-process material (see Radice et al. 2016).

The cross-section of these interactions is proportional to the impact parameter squared and we can determine the relative rates between collisions and mergers from dynamical interactions by taking the ratio of these cross sections. Assuming we need periastron values below 20 km, the frequency ratio of collisions relative to mergers is about 4×10^{-8}. Figure 14 shows the periastron separation as a function of the impact parameter for different values of impact velocities. The rate of eccentric neutron star binaries (or collisions) is extremely rare and, overall, these systems are not expected to contribute significantly to the production of r-process material.

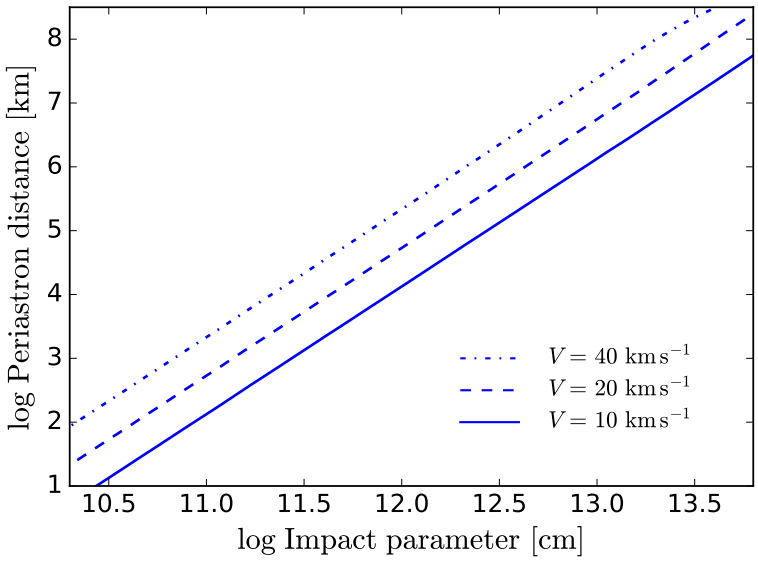

FIG. 14.— Periastron distance as a function of the impact parameter for different impact velocities.